Chapter 3

Linear Lifting Schemes: Interpolative and Projection-based Lifting

3.1 Introduction

Despite of the amount of research effort dedicated to lifting filters optimization (cf. §2.3.2), many works [Li05, Ger05, Hat05] keep on appearing that contribute ideas to improve existing lifting schemes with new optimization criteria and algorithms. Certainly, there is room for contributions, specially in space-varying, signal-dependant, and adaptive lifting. Even in the linear setting, there are several ideas that have not been studied enough. This chapter aims to propose, describe, analyze, and experimentally test linear LS.

The chapter is divided in two approaches, different but intimately related. The first one §3.2 is based on adaptive quadratic interpolation. The method follows the line of work established by Muresan and Parks in [Mur04]. The main objective of [Mur04] is distant from the wavelet domain. The goal is the interpolation of images for digital cameras with any rational degree of zooming. Here, the principal idea of the work is taken up again and further developed in such a way that it serves to create a variety of interpolative PLS. The second approach §3.3 is a projection-based construction of lifting steps, which has some similarities to that of Deever and Hemami [Dee03] in its initial development. The name *projection-based* refers to the interpretation of the simplest prediction step arising from the approach. The optimal result minimizes the projection error of the wavelet basis vector onto the subspace spanned by the scaling basis vectors. New prediction and update lifting steps are derived using this method.

The interpolation-based approach is suited for the construction of space-varying schemes, since it may be locally adaptive. The method searches a (local) optimal interpolation. Meanwhile, the projection-based approach seems more suited for signal-class adapted lifting construction. The filter is optimized for a certain class of images and then it is employed whenever an image belonging to the class is coded.

The advances and results arising from one scheme may be applied to the other one. This is possible because in spite of the different point of departure of each approach, the underlying mathematics are essentially the same for both cases. However, the information mainly flows one-way: from the interpolation to the projection-based approach.

Experiments concerning linear lifting steps construction employing both approaches are elaborated and described in section 3.4. Finally, chapter summary and some conclusions are provided in section 3.5.

Chapter Notation

The notation for this chapter slightly differs from the rest of the dissertation. Let $\mathbf{l}$ ($\cong \mathbf{x}'$) and $\mathbf{h}$ ($\cong \mathbf{y}'$) be the scaling and wavelet coefficients, respectively. The notation stands for low-pass and high-pass, and this is licit because the filters developed in this chapter are linear and despite the fact they are not always strictly band-pass filters. This notation is consistent and makes the exposition clearer. Next chapters address nonlinear LS and the notation introduced in chapter 2 is retaken. The multi-resolution decomposition is

$$\mathbf{x} \rightarrow (\mathbf{l}, \mathbf{h}) = (\mathbf{l}^{(1)}, \mathbf{h}^{(1)}) \rightarrow (\mathbf{l}^{(2)}, \mathbf{h}^{(2)}, \mathbf{h}) \rightarrow \ldots \rightarrow (\mathbf{l}^{(K)}, \mathbf{h}^{(K)}, \mathbf{h}^{(K-1)}, \ldots, \mathbf{h}). \tag{3.1}$$

The decomposition has intermediate $\mathbf{l}$ and $\mathbf{h}$ subsignals not present in the previous multi-resolution representation (3.1). These subsignals are the output of each of the L lifting steps required for the wavelet decomposition. Lifting is defined as the algorithm with the following steps. Super-indexes that indicate the resolution level are omitted for conciseness.

(a) Lazy wavelet transform of the input data $\mathbf{x}$ into two subsignals:

- An approximation or low-pass signal $\mathbf{l}_0$ formed by the even samples of $\mathbf{x}$.
- A detail or high-pass signal $\mathbf{h}_0$ formed by the odd samples of $\mathbf{x}$.

(b) Lifting steps, $i = 1 \ldots L$.

- Prediction P_i of the detail signal with the $\mathbf{l}_{i-1}$ samples,

$$h_i[n] \quad = \quad h_{i-1}[n] - P_i(\mathbf{l}_{i-1}[n]).$$

- Update U_i of the approximation signal with the $\mathbf{h}_i$ samples,

$$l_i[n] \quad = \quad l_{i-1}[n] + U_i(\mathbf{h}_i[n]).$$

(c) Output data: the transform coefficients $\mathbf{l}_L$ and $\mathbf{h}_L$.

The output signal $\mathbf{l}_L = \mathbf{l}^{(1)}$ may be further decomposed. Since the filters are linear, a usual representation of the steps is

$$\begin{aligned} h_i[n] &= h_{i-1}[n] - \mathbf{p}_i^T \mathbf{l}_{i-1}, \\ l_i[n] &= l_{i-1}[n] + \mathbf{u}_i^T \mathbf{h}_i, \end{aligned}$$

where $\mathbf{l}_i = \mathbf{l}_i[n]$ and $\mathbf{h}_i = \mathbf{h}_i[n]$ are column vectors containing an appropriate subset of the subsignals centered at sample n. This chapter is dedicated to the optimization of $\mathbf{p}_1$, $\mathbf{p}_2$, $\mathbf{u}_1$, and $\mathbf{u}_L$. Indexes are omitted for short when they are clear from the context.

3.1.1 Convex Optimization Theory

The theory of convex optimization is applied in this chapter. This theory provides a general framework for solving many constrained optimization problems. The key mathematical reference on the subject is [Roc71]. Two excellent references from a practical implementation perspective with engineering applications are [Ber99] and [Boy04]. The main advantage of convex optimization theory is that closed-form solutions can be found to many problems under some mild conditions based on the application of the Karush-Kuhn-Tucker (KKT) conditions [Boy04, p. 243]. In the case that a closed-form solution does not exist or may not be found, the solution to a convex optimization problem can always be calculated by applying efficient numerical methods. Currently, there exists a wide range of algorithms and public software packages that solve any kind of convex problem in an admissible period of time.

The rest of the section is a brief preliminary on convex optimization, which is useful for the understanding of some mathematical developments throughout the chapter.

A set $\mathcal{D}$ is a convex set if the line segment between any two points in the set lies in the set. This may be expressed mathematically as

$$\alpha \mathbf{x}_1 + (1-\alpha)\mathbf{x}_2 \in \mathcal{A}, \quad \forall \mathbf{x}_1, \mathbf{x}_2 \in \mathcal{D}, \quad \forall \alpha \in [0,1].$$

Similarly, a real-valued function f is a convex function if its domain $\mathcal{D}$ is a convex set and the following inequality holds:

$$f\left(\alpha \mathbf{x}_1 + (1-\alpha)\mathbf{x}_2\right) \leq \alpha f(\mathbf{x}_1) + (1-\alpha) f(\mathbf{x}_2), \quad \forall \mathbf{x}_1, \mathbf{x}_2 \in \mathcal{D}, \quad \forall \alpha \in [0,1],$$

which means that the line segment between $(\mathbf{x}_1, f(\mathbf{x}_1))$ and $(\mathbf{x}_2, f(\mathbf{x}_2))$ lies above the graph of f. A general expression of a constrained optimization problem is

$$\begin{array}{lll} \underset{\mathbf{x}}{\text{minimize}} & f_0(\mathbf{x}) & \\ \text{subject to} & f_i(\mathbf{x}) \leq 0, & 1 \leq i \leq m, \\ & h_i(\mathbf{x}) = 0, & 1 \leq i \leq p, \end{array} \tag{3.2}$$

which consists in finding the infimum of the function $f_0(\mathbf{x})$ (which is called the objective function) among all $\mathbf{x}$ that satisfy the conditions $f_i(\mathbf{x}) \leq 0,\ i = 1, \ldots, m$, and $h_i(\mathbf{x}) = 0,\ i = 1, \ldots, p$, simultaneously.

The optimization variable is $\mathbf{x}$. The inequality constraints and inequality constraint functions are $f_i(\mathbf{x}) \leq 0$ and $f_i(\mathbf{x})$, respectively. Finally, the equality constraints and equality constraint functions are $h_i(\mathbf{x}) = 0$ and $h_i(\mathbf{x})$, respectively. The set of points for which the objective and all the constraint functions are defined is called the domain of the optimization problem (3.2).

The problem (3.2) is a convex optimization problem if the objective function and the inequality constraint functions are convex, and if the equality constraint functions are affine, i.e., $h_i(\mathbf{x}) = \mathbf{a}_i^T\mathbf{x} + b_i$. This definition implies that the domain of the optimization problem is convex. The optimal value $f^\star$ of the problem is defined as

$$f^\star \triangleq \inf \{f_0(\mathbf{x}) : f_i(\mathbf{x}) \leq 0,\ i = 1, \ldots, m,\ h_i(\mathbf{x}) = 0,\ i = 1, \ldots, p\}\,. \tag{3.3}$$

The KKT conditions is a way that provides the convex optimization theory to obtain the optimal solution. A previous requirement is to define the Lagrangian function L associated to the problem,

$$L(\mathbf{x}; \boldsymbol{\lambda}, \boldsymbol{\nu}) \triangleq f_0(\mathbf{x}) + \sum_{i=1}^{m} \lambda_i f_i(\mathbf{x}) + \sum_{i=1}^{p} \nu_i h_i(\mathbf{x}), \tag{3.4}$$

where $\boldsymbol{\lambda} = (\lambda_1 \cdots \lambda_m)^T$ and $\boldsymbol{\nu} = (\nu_1 \cdots \nu_p)^T$ are the Lagrange multipliers vectors. In the case that all the functions are differentiable and under some other technical conditions, a set of expressions have to be fulfilled by any optimal solution $\mathbf{x}^\star$ and optimal Lagrangian variables $(\boldsymbol{\lambda}^\star, \boldsymbol{\nu}^\star)$. The expressions are the so-called KKT conditions:

$$\begin{aligned}
h_i(\mathbf{x}^\star) &= 0, \quad i = 1, \ldots, p, \\
f_i(\mathbf{x}^\star) &\leq 0, \quad i = 1, \ldots, m, \\
\lambda_i^\star &\geq 0, \quad i = 1, \ldots, m, \\
\lambda_i^\star f_i(\mathbf{x}^\star) &= 0, \quad i = 1, \ldots, m, \\
\nabla f_0(\mathbf{x}^\star) + \sum_{i=1}^{m} \lambda_i^\star \nabla f_i(\mathbf{x}^\star) + \sum_{i=1}^{p} \nu_i^\star \nabla h_i(\mathbf{x}^\star) &= \mathbf{0}.
\end{aligned}$$

Some of the problems that appear in this chapter are formulated as quadratic programs, in which the objective function is convex quadratic and all the equality and inequality constraint functions are affine. KKT conditions are used to solve them, giving a closed-form solution. Some other problems are reduced to linear programs, in which all functions $f_i,\ i = 0, \ldots, m$, and $h_i,\ i = 1, \ldots, p$, are affine and for which convex optimization provides simple and efficient numerical algorithms to obtain a solution.

3.2 Quadratic Image Interpolation Methods

This section presents an interpolation method based on adaptively determining the quadratic signal class from the local image behavior. The interpolation method has the ability to interpolate by any rational factor and to model properties of the image acquisition device or other external constraints into the algorithm itself.

In [Mur04], a quadratic signal model is established and then the interpolation is found by means of the optimal recovery theory [Mic76, Mur02]. Our study of this method has revealed that the problem can be reformulated as the minimization of a quadratic function with linear equality constraints. This insight provides us with all the resources and flexibility coming from the convex optimization theory in order to solve the problem. Furthermore, the initial problem statement may be modified in many ways and convex optimization theory still offers solutions. For instance, equality and inequality constraints on the smoothness of the signal or on its lower and upper bounds may be included.

The new found flexibility is employed in section 3.3 to design lifting steps with different criteria from the usual vanishing moments or spectral considerations. However, an interpolative PLS may be constructed directly. The interpolation values may be used as the prediction of the detail samples. Also, the interpolation value may be a basis reference of the image underlying probability density function for an optimized prediction. The prediction may be considered the peak value of a mono-modal symmetrical distribution of the sample (cf. §5.1.2).

3.2.1 Quadratic Interpolation

The adaptive interpolation method is based on two steps. First, a set to which the signal belongs or a signal model is determined. Second, the interpolation that best fits the model given the local signal is found.

A quadratic signal class $\mathcal{K}$ is defined as

$$\mathcal{K} = \{\mathbf{x} \in \mathbb{R}^n : \mathbf{x}^T\mathbf{Q}\mathbf{x} \leq \epsilon\}.$$

The choice of a quadratic model is practical because it can be determined easily by a set of training data and also, because an appropriate choice of matrix $\mathbf{Q}$ facilitates the derivation of the optimal interpolation values.

The training data is taken from the local features of the image. Alternatively, it is taken from images of the same type or from any image model. Assume that a training set of patches $\mathcal{S} = \{x_1, \ldots, x_m\}$ representative of the local data is given for estimating the local quadratic signal class. Then, matrix $\mathbf{Q}$ defines an ellipsoid

$$\mathbf{x}^T\mathbf{Q}\mathbf{x} \leq \epsilon \tag{3.5}$$

that must be representative of the training set $\mathcal{S}$ for some constant ϵ. In other words, $\mathbf{Q}$ must be a matrix such that when an image patch $\mathbf{y}$ is similar to the vectors in $\mathcal{S}$, then (3.5) holds for $\mathbf{y}$. Let matrix $\mathbf{S}$ be formed by arranging the image patches in $\mathcal{S}$ as columns

$$\mathbf{S} = (\mathbf{x}_1 \dots \mathbf{x}_m),$$

and consider the equation relating the image patch $\mathbf{y}$ to the training set $\mathcal{S}$ using a column vector $\mathbf{c}$ formed of m weights,

$$\mathbf{Sc} = \mathbf{y}.$$

Vector $\mathbf{y}$ lies in the expansion of the columns of $\mathbf{S}$. Therefore, $\mathbf{y}$ is similar to the vectors in $\mathbf{S}$ when $\mathbf{c}$ has small energy,

$$\|\mathbf{c}\|^2 = \mathbf{c}^T\mathbf{c} = \mathbf{y}^T(\mathbf{S}\mathbf{S}^T)^{-1}\mathbf{y} = \mathbf{y}^T\mathbf{Q}\mathbf{y} \leq \epsilon,$$

where $\mathbf{Q}$ is the pseudo-inverse of the product matrix $\mathbf{S}\mathbf{S}^T$. In this sense, good interpolators of $\mathbf{y}$ for the quadratic class determined by $\mathbf{Q}$ are spanned with the weighting vectors $\mathbf{c}$ of energy bounded with some ϵ.

The training set has to be determined. One direct approach of selecting the elements in $\mathcal{S}$ is based on the proximity of their locations to the position of the vector being modeled. In this case, patches are generated from the local neighborhood. For example, in figure 3.1 the center patch

$$\mathbf{x} = (x_{(2,2)}\ x_{(2,3)}\ x_{(2,4)}\ x_{(2,5)}\ x_{(3,2)}\ \dots\ x_{(5,5)})^T$$

may be modeled by the quadratic signal class of the set

$$\mathcal{S} = \left\{ \begin{pmatrix} x_{(0,0)} \\ x_{(0,1)} \\ \vdots \\ x_{(3,3)} \end{pmatrix}, \dots, \begin{pmatrix} x_{(4,4)} \\ x_{(4,5)} \\ \vdots \\ x_{(7,7)} \end{pmatrix} \right\},$$

where $\mathcal{S}$ is formed by choosing all the possible 4x4 image blocks in the 8x8 region of the figure.

3.2.2 Optimal Quadratic Interpolation

Once the high density class $\mathcal{K}$ has been determined, the optimal interpolation vector $\mathbf{x}$ can be expressed as the solution of a convex optimization problem (3.2). We are looking for the minimum energy vector $\mathbf{c}$ subject to the constraint that $\mathbf{x}$ is a linear combination of the selected image patches. This statement can be formulated as

$$\begin{aligned} \underset{\mathbf{x},\mathbf{c}}{\text{minimize}} \quad & \|\mathbf{c}\|^2 \\ \text{subject to} \quad & \mathbf{Sc} = \mathbf{x}. \end{aligned} \tag{3.6}$$

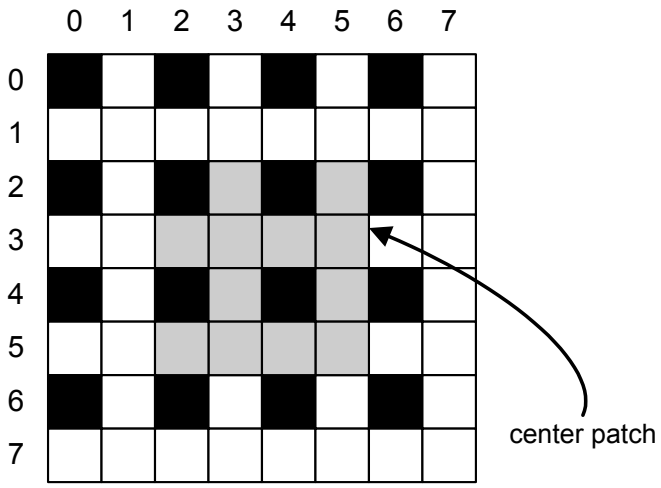

Figure 3.1: Local high density image used for selecting $\mathcal{S}$ to estimate the quadratic class for the center 4x4 patch (dark pixels are part of the decimated image).

The optimal solution of (3.6) is $\mathbf{x}^\star = \mathbf{0}$ and $\mathbf{c}^\star = \mathbf{0}$. The information coming from the interpolated signal should be included in the formulation to obtain meaningful solutions.

Previous knowledge about $\mathbf{x}$ is available since only some of its components have to be interpolated. Typically, if a decimation by two has been performed in both image directions, then one of every four elements of $\mathbf{x}$ are already known. Also, it may be known that the original high density signal has been averaged before the decimation. In both cases, a linear constraint on the data is known and it may be added to the formulation (3.6). The linear constraint is denoted by $\mathbf{A}^T\mathbf{x} = \mathbf{b}$. In the first case, the columns of matrix $\mathbf{A}$ are formed by vectors $\mathbf{e}_i$, being the one located at the position of the known sample. The respective position of vector $\mathbf{b}$ has the value of the sample. An illustrative example for the second case is the following. Assume that the pixel value is the average of four high density neighbors, then there would be 1/4 at each of their corresponding positions in a column of $\mathbf{A}$. Whatever the linear constraints, they are included in (3.6) to reach the formulation,

$$\begin{array}{ll} \underset{\mathbf{x},\mathbf{c}}{\text{minimize}} & \|\mathbf{c}\|^2 \\ \text{subject to} & \mathbf{S}\mathbf{c} = \mathbf{x}, \\ & \mathbf{A}^T\mathbf{x} = \mathbf{b}. \end{array} \tag{3.7}$$

This formulation is mathematically equivalent to that of [Mur04] but the convex form allows an easier interpretation and resolution, as well as the variety of alternative formulations provided in §3.2.3 and the modification in order to design lifting steps explained in §3.3.

The solution of the problem (3.7) is

$$\mathbf{x}^\star = \mathbf{S}\mathbf{S}^T\mathbf{A}(\mathbf{A}^T\mathbf{S}\mathbf{S}^T\mathbf{A})^{-1}\mathbf{b}, \tag{3.8}$$

which is the least-square solution with the quadratic norm determined by $\mathbf{S}\mathbf{S}^T$ and the linear constraints $\mathbf{A}^T\mathbf{x} = \mathbf{b}$. The vector

$$\mathbf{c}^\star = \mathbf{S}^T\mathbf{A}(\mathbf{A}^T\mathbf{S}\mathbf{S}^T\mathbf{A})^{-1}\mathbf{b} = \tilde{\mathbf{A}}(\tilde{\mathbf{A}}^T\tilde{\mathbf{A}})^{-1}\mathbf{b} \tag{3.9}$$

that minimizes the expected energy of $\mathbf{c}$ corresponds to an orthogonal projection of $\mathbf{0}$ onto the subspace $\bar{\mathbf{S}}$ spanned by $\tilde{\mathbf{A}} = \mathbf{S}^T\mathbf{A}$.

The matrix $\mathbf{S}\mathbf{S}^T$ is symmetric and positive definite. This fact makes the optimization problem convex. In the example given by figure 3.1, matrix $\mathbf{S}\mathbf{S}^T$ is

$$\begin{aligned}
\mathbf{S}\mathbf{S}^T &= \left(\begin{pmatrix} x_{(0,0)} \\ x_{(0,1)} \\ \vdots \\ x_{(3,3)} \end{pmatrix} \cdots \begin{pmatrix} x_{(4,4)} \\ x_{(4,5)} \\ \vdots \\ x_{(7,7)} \end{pmatrix} \right) \begin{pmatrix} \left(x_{(0,0)}\ x_{(0,1)}\ \cdots\ x_{(3,3)}\right) \\ \vdots \\ \left(x_{(4,4)}\ x_{(4,5)}\ \cdots\ x_{(7,7)}\right) \end{pmatrix} \\
&= \begin{pmatrix} \sum_{\mathbf{k}=(0,0)}^{(4,4)} x_{\mathbf{k}}^2 & \sum_{\mathbf{k}} x_{\mathbf{k}} x_{\mathbf{k}+(0,1)} & \cdots & \sum_{\mathbf{k}} x_{\mathbf{k}} x_{\mathbf{k}+(4,4)} \\ \sum_{\mathbf{k}=(0,1)}^{(4,5)} x_{\mathbf{k}} x_{\mathbf{k}-(0,1)} & \sum_{\mathbf{k}} x_{\mathbf{k}}^2 & \cdots & \sum_{\mathbf{k}} x_{\mathbf{k}} x_{\mathbf{k}+(4,3)} \\ \vdots & \vdots & \ddots & \vdots \\ \sum_{\mathbf{k}=(4,4)}^{(7,7)} x_{\mathbf{k}} x_{\mathbf{k}-(4,4)} & \cdots & \cdots & \sum_{\mathbf{k}} x_{\mathbf{k}}^T \end{pmatrix} \propto \hat{\mathbf{R}},
\end{aligned}$$

which is proportional to an estimation of the local image auto-correlation. The proportionality factor is not annoying because it appears in $\mathbf{S}\mathbf{S}^T$ and in the inverse $(\mathbf{A}^T\mathbf{S}\mathbf{S}^T\mathbf{A})^{-1}$ of equation (3.8), so it is canceled out.

The formulation is made "global" by interpreting the image signal as a discrete-random process and taking the expectation in (3.8). In this case, the quadratic class is determined by the correlation matrix $\mathbf{R} = \mathbb{E}\left[\mathbf{S}\mathbf{S}^T\right]$. The corresponding solution is

$$\mathbf{x}^\star = \mathbf{R}\mathbf{A}(\mathbf{A}^T\mathbf{R}\mathbf{A})^{-1}\mathbf{b}, \tag{3.10}$$

which is the least-squares solution of the norm determined by $\mathbf{R}$ and the constraints $\mathbf{A}^T\mathbf{x} = \mathbf{b}$, i.e., the solution of

$$\begin{aligned} \underset{\mathbf{x}}{\text{minimize}} \quad & \mathbf{x}^T\mathbf{R}^{-1}\mathbf{x} \\ \text{subject to} \quad & \mathbf{A}^T\mathbf{x} = \mathbf{b}. \end{aligned}$$

Note that $\mathbf{R}$ is an auto-correlation matrix, which is symmetric and positive definite and so the optimization problem is still convex. There are many ways to extract an estimation of the correlation matrix from the image data: the biased or unbiased estimators, with pre-windowing or not, the auto-regressive parametric models, etc. The image data may even be a region segmented from an image, the entire image, a whole image class, etc. The choice of the estimation method and the signal data depends on the application at hand.

Local adapted and global interpolative predictions may be constructed with this common formulation. Additional knowledge is easily included in the formulation thanks to its flexibility.

In the next subsection, several alternative formulations that modify the original in different ways are proposed.

Another consideration is that the proposed interpolation methods give solution vectors that can be seen as new data patches, better in some sense than the originally used by the algorithm. Therefore, these solution vectors may also be provided to a subsequent iteration of the algorithm, thus improving initial results.

3.2.3 Alternative Formulations

The initial formulation (3.7) solution gives a good interpolation, which is optimal in the specified sense. However, the problem statement may be further refined including more available knowledge, from the local data or from the given application. Knowledge is introduced in the formulation by modifying the objective function or by adding new constraints to the existing ones. Different alternative formulations are described in the following.

3.2.3.1 Signal Bound Constraint

The data from an image is expressed with a certain number of bits, lets say *nbits* bits. Then, assume without loss of generality that the value of any component of $\mathbf{x}$ is low-bounded by 0 and up-bounded by $2^{nbits} - 1$. This is an additional constraint that is included in the problem statement,

$$\begin{array}{ll} \underset{\mathbf{x},\mathbf{c}}{\text{minimize}} & \|\mathbf{c}\|^2 \\ \text{subject to} & \mathbf{S}\mathbf{c} = \mathbf{x}, \\ & \mathbf{A}^T\mathbf{x} = \mathbf{b}, \\ & \mathbf{0} \leq \mathbf{x} \leq (2^{nbits} - 1) \cdot \mathbf{1}, \end{array} \tag{3.11}$$

where $\mathbf{0}$ ($\mathbf{1}$) is the column vector of the size of $\mathbf{x}$ containing all zeros (ones). The symbol $\leq$ indicates elementwise inequality. Let us define the set

$$\mathcal{D} = \{\mathbf{x} \in \mathbb{R}^n \mid \mathbf{0} \leq \mathbf{x} \leq (2^{nbits} - 1) \cdot \mathbf{1}\}.$$

Notice that (3.11) is a quadratic problem with inequality linear constraints and so, it has no closed-form solution. Anyway, there exist efficient numerical algorithms and widespread software packages that attain the optimal solution very fast. Nevertheless, if the optimal solution $\mathbf{x}^\star$ of (3.11) resides in the bounded domain $\mathcal{D}$, then this is the closed-form solution expressed by (3.10). If the set of patches and linear equality constraints have been correctly chosen, then $\mathbf{x}^\star$ is almost always in the hypercube $\mathcal{D}$.

3.2.3.2 Weighted Objective

Another refinement of (3.7) is the weighting of vector $\mathbf{c}$ in order to give more importance to the local signal patches that are closer to $\mathbf{x}$. Closer patches are supposed to be more alike than the further ones. The formulation is

$$\begin{array}{ll} \underset{\mathbf{x},\mathbf{c}}{\text{minimize}} & \|\tilde{\mathbf{W}}\mathbf{c}\|^2 \\ \text{subject to} & \mathbf{S}\mathbf{c} = \mathbf{x}, \\ & \mathbf{A}^T\mathbf{x} = \mathbf{b}, \end{array}$$

where $\tilde{\mathbf{W}}$ is a diagonal matrix with the weighting elements w_{ii} related to the distance of the corresponding patch (in the column i of $\mathbf{S}$) to the patch $\mathbf{x}$. Let define $\mathbf{W} = \tilde{\mathbf{W}}^T\tilde{\mathbf{W}}$, then the problem may be reformulated as

$$\begin{array}{ll} \underset{\mathbf{c}}{\text{minimize}} & \mathbf{c}^T\mathbf{W}\mathbf{c} \\ \text{subject to} & \mathbf{A}^T\mathbf{S}\mathbf{c} = \mathbf{b}, \end{array}$$

which is solved using the KKT conditions:

$$\text{KKT conditions: } \left\{ \begin{array}{l} \mathbf{A}^T\mathbf{S}\mathbf{c} - \mathbf{b} = \mathbf{0} \\ 2\mathbf{W}\mathbf{c} + \mathbf{S}^T\mathbf{A}\mu = \mathbf{0} \end{array} \right. \cong \begin{pmatrix} \mathbf{A}^T\mathbf{S} & \mathbf{0} \\ 2\mathbf{W} & \mathbf{S}^T\mathbf{A} \end{pmatrix} \begin{pmatrix} \mathbf{c} \\ \mu \end{pmatrix} = \begin{pmatrix} \mathbf{b} \\ \mathbf{0} \end{pmatrix}. \tag{3.12}$$

Matrix on the RHS of expression (3.12) equivalence sign is invertible, so it is straightforward to compute the optimal vectors $\mathbf{c}^\star$ and $\mathbf{x}^\star$,

$$\begin{aligned} \mathbf{c}^\star &= \mathbf{W}^{-1}\mathbf{S}^T\mathbf{A}(\mathbf{A}^T\mathbf{S}\mathbf{W}^{-1}\mathbf{S}^T\mathbf{A})^{-1}\mathbf{b}, \\ \mathbf{x}^\star &= \mathbf{S}\mathbf{W}^{-1}\mathbf{S}^T\mathbf{A}(\mathbf{A}^T\mathbf{S}\mathbf{W}^{-1}\mathbf{S}^T\mathbf{A})^{-1}\mathbf{b}. \end{aligned} \tag{3.13}$$

The solution (3.13) corresponds to the orthogonal projection of $\mathbf{0}$ onto the subspace spanned by $\tilde{\mathbf{W}}^{-1}\mathbf{S}^T\mathbf{A}$. The initial projection subspace $\mathbf{S}^T\mathbf{A}$ is modified according to the weight given to each of the patches.

3.2.3.3 Energy Penalizing Objective

A possible modification of (3.7) is to limit vector $\mathbf{x}$ energy by introducing a penalizing factor in the objective function. The two objectives are merged through a parameter γ that balances their importance. The resulting formulation is

$$\begin{array}{ll} \underset{\mathbf{x},\mathbf{c}}{\text{minimize}} & \gamma\|\tilde{\mathbf{W}}\mathbf{c}\|^2 + (1-\gamma)\|\mathbf{x}\|^2 \\ \text{subject to} & \mathbf{S}\mathbf{c} = \mathbf{x}, \\ & \mathbf{A}^T\mathbf{x} = \mathbf{b}, \end{array} \tag{3.14}$$

which is equivalent to

$$\begin{array}{ll} \underset{\mathbf{x},\mathbf{c}}{\text{minimize}} & \begin{pmatrix} \mathbf{c}^T & \mathbf{x}^T \end{pmatrix} \begin{pmatrix} \gamma\mathbf{W} & \mathbf{0} \\ \mathbf{0} & (1-\gamma)\mathbf{I} \end{pmatrix} \begin{pmatrix} \mathbf{c} \\ \mathbf{x} \end{pmatrix} \\ \text{subject to} & \begin{pmatrix} \mathbf{0} & \mathbf{A}^T \\ \mathbf{S} & -\mathbf{I} \end{pmatrix} \begin{pmatrix} \mathbf{c} \\ \mathbf{x} \end{pmatrix} = \begin{pmatrix} \mathbf{b} \\ \mathbf{0} \end{pmatrix}. \end{array} \tag{3.15}$$

The variables to minimize are $\mathbf{c}$ and $\mathbf{x}$. All the constraints are linear with equality. KKT conditions are established. If there are l linear constraints because of $\mathbf{A}^T\mathbf{x} = \mathbf{b}$ and m local patches in $\mathcal{S}$, then the resulting linear system derived from the KKT conditions is

$$\begin{pmatrix} \mathbf{0}_{l\times m} & \mathbf{A}^T & \mathbf{0}_{l\times l} & \mathbf{0}_{l\times n} \\ \mathbf{S} & -\mathbf{I}_n & \mathbf{0}_{n\times l} & \mathbf{0}_{n\times n} \\ 2\gamma\mathbf{W} & \mathbf{0}_{m\times n} & \mathbf{0}_{m\times l} & \mathbf{S}^T \\ \mathbf{0}_{n\times m} & 2(1-\gamma)\mathbf{I}_n & \mathbf{A} & -\mathbf{I}_n \end{pmatrix} \begin{pmatrix} \mathbf{c} \\ \mathbf{x} \\ \mu \end{pmatrix} = \begin{pmatrix} \mathbf{b} \\ \mathbf{0}_{(2n+m)\times 1} \end{pmatrix},$$

where $\mu \in \mathbb{R}^{l+n}$. The system matrix is invertible if the chosen $\mathbf{W}$ is invertible. Then, the solution reduces to

$$\mathbf{x}^\star = \begin{cases} \mathbf{A}(\mathbf{A}^T\mathbf{A})^{-1}\mathbf{b}, & \text{if} \quad \gamma = 0, \\ (\mathbf{I}-\mathbf{F}^{-1})\mathbf{A}(\mathbf{A}^T(\mathbf{I}-\mathbf{F}^{-1})\mathbf{A})^{-1}\mathbf{b}, & \text{if} \quad 0 < \gamma < 1, \\ \mathbf{S}\mathbf{W}^{-1}\mathbf{S}^T\mathbf{A}(\mathbf{A}^T\mathbf{S}\mathbf{W}^{-1}\mathbf{S}^T\mathbf{A})^{-1}\mathbf{b}, & \text{if} \quad \gamma = 1, \end{cases}$$

where $\mathbf{F}$ is introduced to make the expression clearer,

$$\mathbf{F} = \frac{1-\gamma}{\gamma}\mathbf{S}\mathbf{W}^{-1}\mathbf{S}^T + \mathbf{I}.$$

Parameter γ balances the weight of each criterion. If $\gamma = 0$, then the solution is the least-squares onto the linear subspace defined by the constraints $\mathbf{A}^T\mathbf{x} = \mathbf{b}$. On the other hand, the energy of $\mathbf{x}$ has no relevance for $\gamma = 1$, and the solution reduces to (3.13). Intermediate solutions are obtained for $0 < \gamma < 1$.

3.2.3.4 Signal Regularizing Objective

An interesting refinement is to include a regularization factor as part of the objective function. Let define the differential matrix $\mathbf{D}$, which computes the differences between elements of $\mathbf{x}$. Typically, rows of $\mathbf{D}$ are all zeros except a 1 and a -1 corresponding to positions of neighboring data, i.e., neighboring samples in a 1-D signal or neighboring pixels in an image. The minimization of the differences vector $\mathbf{D}\mathbf{x}$ energy leads to smooth interpolations. The new problem statement is

$$\begin{aligned} \underset{\mathbf{x},\mathbf{c}}{\text{minimize}} \quad & \|\tilde{\mathbf{W}}\mathbf{c}\|^2 + \delta\|\mathbf{D}\mathbf{x}\|^2 \\ \text{subject to} \quad & \mathbf{S}\mathbf{c} = \mathbf{x}, \\ & \mathbf{A}^T\mathbf{x} = \mathbf{b}. \end{aligned}$$

As before, the expression can be redefined in a more useful way to derive the KKT conditions. The constraints are the same as (3.15), while the objective function is

$$\begin{pmatrix} \mathbf{c}^T & \mathbf{x}^T \end{pmatrix} \begin{pmatrix} \mathbf{W} & \mathbf{0} \\ \mathbf{0} & \delta\mathbf{D}^T\mathbf{D} \end{pmatrix} \begin{pmatrix} \mathbf{c} \\ \mathbf{x} \end{pmatrix}.$$

Therefore, the linear equations system

$$\begin{pmatrix} \mathbf{0}_{l\times m} & \mathbf{A}^T & \mathbf{0}_{l\times l} & \mathbf{0}_{l\times n} \\ \mathbf{S} & -\mathbf{I}_n & \mathbf{0}_{n\times l} & \mathbf{0}_{n\times n} \\ 2\mathbf{W} & \mathbf{0}_{m\times n} & \mathbf{0}_{m\times l} & \mathbf{S}^T \\ \mathbf{0}_{n\times m} & 2\delta\mathbf{D}^T\mathbf{D} & \mathbf{A} & -\mathbf{I}_n \end{pmatrix} \begin{pmatrix} \mathbf{c} \\ \mathbf{x} \\ \mu \end{pmatrix} = \begin{pmatrix} \mathbf{b} \\ \mathbf{0}_{(2n+m)\times 1} \end{pmatrix} \tag{3.16}$$

has to be solved. The system has a unique solution if $\mathbf{W}$ and $\mathbf{D}^T\mathbf{D}$ are invertible matrices. $\mathbf{W}$ is a weight matrix chosen to be full rank. However, $\mathbf{D}^T\mathbf{D}$ is singular as defined because any constant vector belongs to the kernel of the matrix (since it is the product of two differential matrices). It may be made full rank by diagonal loading or by adding a constant row to $\mathbf{D}$. The latter option has the advantage to introduce the energy weighting factor of (3.14) in the formulation. More or less weight is given to the energy criterion depending on the value of the constant row. Whatever the choice, the optimal solution is

$$\mathbf{x}^\star = \mathbf{M}(\mathbf{I} - \mathbf{F}^{-1}\mathbf{M})\mathbf{A}(\mathbf{A}^T\mathbf{M}(\mathbf{I} - \mathbf{F}^{-1}\mathbf{M})\mathbf{A})^{-1}\mathbf{b}, \tag{3.17}$$

where $\mathbf{M} = (\mathbf{D}^T\mathbf{D})^{-1}$. In general, $\mathbf{F}$ is an invertible matrix and it is defined as

$$\mathbf{F} = \delta\mathbf{S}\mathbf{W}^{-1}\mathbf{S}^T + \mathbf{M}.$$

3.2.3.5 l^1-norm Objective

Other norms than the Euclidean may be considered. The l^1-norm may be used to force the components of a vector to sum up to a constant by minimizing the absolute value of the difference between the components sum and the constant. For instance, if the elements of vector $\mathbf{c}$ are forced to sum up as close as possible to one, then it is assured that the energy of the solution is similar to that of the patches, which is certainly a desired property in the case of stationary signals. The problem statement reduces to

$$\begin{array}{ll} \underset{\mathbf{x},\mathbf{c}}{\text{minimize}} & |\mathbf{1}^T\mathbf{c} - 1| \\ \text{subject to} & \mathbf{A}^T\mathbf{x} = \mathbf{b}, \\ & \mathbf{S}\mathbf{c} = \mathbf{x}, \end{array} \quad \cong \quad \begin{array}{ll} \underset{\mathbf{x}}{\text{minimize}} & |\mathbf{1}^T\mathbf{S}^{\#}\mathbf{x} - 1| \\ \text{subject to} & \mathbf{A}^T\mathbf{x} = \mathbf{b}, \end{array}$$

where $\mathbf{S}^{\#} = (\mathbf{S}^T\mathbf{S})^{-1}\mathbf{S}^T$. The function seems difficult to optimize, but the problem may be put as the equivalent linear program

$$\begin{array}{ll} \underset{\mathbf{x},t}{\text{minimize}} & t \\ \text{subject to} & \mathbf{1}^T\mathbf{S}^{\#}\mathbf{x} - 1 \leq t, \\ & \mathbf{1}^T\mathbf{S}^{\#}\mathbf{x} - 1 \geq t, \\ & \mathbf{A}^T\mathbf{x} = \mathbf{b}. \end{array}$$

The problem is reduced to a linear program: it has a linear objective function and linear constraints. A linear program is efficiently solved by many numerical methods, as for example, the simplex method. Linear programs are simple problems within the convex optimization theory.

The use of l^1-norms may be mixed with the previously proposed refinements for the quadratic case as long as the added objectives are l^1-norms. The resulting programs are also linear and thus, easily solvable.

3.3 Projection-based Lifting

This section takes up again the formulation (3.7) adding linear equality constraints due to the wavelet coefficients inner product in order to create lifting steps. The formulation may be used for the construction of local adapted as well as global interpolative predictions. Remarkably, the same formulation introducing the new linear equality constraints permits the construction of PLS §3.3.2 that are not the first one and also ULS §3.3.3. Therefore, this common formulation is able to deal with three different problems: interpolation and prediction and update lifting steps design. Experiments in §3.4 provide results for the obtained lifting steps.

3.3.1 Wavelet Linear Constraint

The linear constraint on the data may have a different meaning than the ones established in the previous section. It has been assumed that the constraint refers to the specific value of a sample or the average of several high density neighbors in order to perform an interpolation.

Assume now that the given data is the wavelet decomposition of a signal. Transformed coefficients are the inner products of wavelet (or scaling) basis vectors $\mathbf{w}_i$ with the input signal. With this notation, coefficients $h[n]$ and $l[n]$ arise from the product $h[n] = \mathbf{w}_{h[n]}^T\mathbf{x}$ and $l[n] = \mathbf{w}_{l[n]}^T\mathbf{x}$, respectively. Then, the linear constraint $\mathbf{A}^T\mathbf{x} = \mathbf{b}$ on the data is constructed in the following way. Columns in matrix $\mathbf{A}$ are formed by the wavelet transform basis vectors $\mathbf{w}_i$ and the independent term $\mathbf{b}$ is formed by the transformed coefficients themselves. Therefore, the formulation

$$\begin{aligned} \underset{\mathbf{x},\mathbf{c}}{\text{minimize}} \quad & \|\mathbf{c}\|^2 \\ \text{subject to} \quad & \mathbf{S}\mathbf{c} = \mathbf{x}, \\ & \mathbf{A}^T\mathbf{x} = \mathbf{b}, \end{aligned}$$

may also be applied if a set of patches $\mathcal{S}$ is available. Indeed, the solution is already known from previous section. The global formulation solution is $\mathbf{x}^\star = \mathbf{R}\mathbf{A}(\mathbf{A}^T\mathbf{R}\mathbf{A})^{-1}\mathbf{b}$ (3.10).

The linear constraint allows an alternative way of estimating the signal auto-correlation through the use of the wavelet transform coefficients. Let $\mathbf{A}$ be a local wavelet basis and $\mathbf{A}^T\mathbf{x} = \mathbf{t}$, being $\mathbf{t}$ a vector containing the transformed coefficients $\mathbf{l}$ and $\mathbf{h}$. Then, the inverse of $\mathbf{A}$ exists, which is the matrix formed of the synthesis wavelet basis vectors. Therefore, the auto-correlation can be expressed as

$$\mathbf{R} = \mathbb{E}[\mathbf{x}\mathbf{x}^T] = \mathbb{E}[\mathbf{A}^{-T}\mathbf{t}\mathbf{t}^T\mathbf{A}^{-1}] = \mathbf{A}^{-T}\mathbb{E}[\mathbf{t}\mathbf{t}^T]\mathbf{A}^{-1} = \mathbf{A}^{-T}\mathbf{R}_t\mathbf{A}^{-1},$$

being $\mathbf{R}_t$ the wavelet transform correlation matrix. Thus, using the available transform coefficients, an estimation of $\mathbf{R}_t$ may be obtained. This estimation may be directly used in some of the presented solutions as in (3.10) because of the equality $\mathbf{R}_t = \mathbf{A}^T\mathbf{R}\mathbf{A}$. Also, the need of computing an inverse matrix twice is avoided.

Now, the goal is to predict (update) a wavelet (scaling) coefficient. These coefficients have been already filtered, so somehow the goal is to improve or refine the lifting steps. First, the prediction case is analyzed in §3.3.2, and afterwards the update case in §3.3.3.

3.3.2 Linear Prediction Steps Construction

A coefficient $h[n]$ is predicted using a set of scaling samples, which are denoted with some notation abuse by $\mathbf{l}[n]$. For the sake of exposition clarity, index n is sometimes omitted in vectors $\mathbf{l}[n]$ and $\mathbf{h}[n]$. The linear constraint independent term vector is $\mathbf{b} = \mathbf{l}$ and the system matrix $\mathbf{A} = \mathbf{W}_\mathbf{l}$, where the notation $\mathbf{W}$ indicates that the matrix columns are wavelet basis vectors.

Using the established notation, a wavelet coefficient is expressed by $h_1[n] = \mathbf{w}_{h_1[n]}^T\mathbf{x}$ and it is predicted with a linear filter such that $\hat{h}_1[n] = \mathbf{p}_2^T\mathbf{b}$. The second prediction step $\mathbf{p}_2$ aims at obtaining a predicted value $h_2[n]$,

$$h_2[n] = h_1[n] - \hat{h}_1[n] = h_1[n] - P_2(\mathbf{l}_1[n]) = h_1[n] - \mathbf{p}_2^T\mathbf{l}_1,$$

that improves the initial detail samples properties in order to compress them. A key observation is that the coefficients $\mathbf{l}_1[n]$ constitute a low-resolution signal version that may be interpolated using any of the derivations of section §3.2. Therefore, an optimal interpolation $\mathbf{x}^\star$ (which is an estimation of $\mathbf{x}$) is used to estimate $h_1[n]$ through the inner product with the known wavelet basis vector $\mathbf{w}_{h_1[n]}$. Thus, the estimated coefficient is

$$\hat{h}_1[n] = \mathbf{w}_{h_1[n]}^T\mathbf{x}^\star. \tag{3.18}$$

The optimal linear prediction filter $\mathbf{p}_2$ arises from developing (3.18) using the expression of $\mathbf{x}^\star$ if a closed-form solution exists. In the case of (3.10), such a development is simply

$$\hat{h}_1[n] = \mathbf{w}_{h_1[n]}^T\mathbf{x}^\star = \mathbf{w}_{h_1[n]}^T\mathbf{R}\mathbf{A}(\mathbf{A}^T\mathbf{R}\mathbf{A})^{-1}\mathbf{b} = \mathbf{p}_2^T\mathbf{b}, \tag{3.19}$$

and so, the underlying second prediction is

$$\mathbf{p}_2^\star = (\mathbf{A}^T\mathbf{R}\mathbf{A})^{-1}\mathbf{A}^T\mathbf{R}\mathbf{w}_{h_1[n]}. \tag{3.20}$$

Interestingly, the optimal prediction filter (3.20) obtained with the use of the optimal interpolation solution (3.7) is the same as the one given by the minimum MSE $\mathbf{p}_2$ filter of (3.21) up to the exact choice of matrix $\mathbf{R}$. The MMSE filter minimizes the energy of the second prediction step $h_2[n] = h_1[n] - \hat{h}_1[n]$,

$$\mathbf{p}_2^\star = \arg\min_{\mathbf{p}_2} f_0(\mathbf{p}_2) = \mathbb{E}[(h_1[n] - \hat{h}_1[n])^2]. \tag{3.21}$$

The following derivation proves that both optimal prediction filters coincide. First, the objective function is developed,

$$\begin{aligned} f_0(\mathbf{p}_2) &= \mathbb{E}[(h_1[n] - \hat{h}_1[n])^2] = \mathbb{E}[(\mathbf{w}_{h_1[n]}^T\mathbf{x} - \mathbf{p}_2^T\mathbf{b})^2] \\ &= \mathbb{E}[\mathbf{w}_{h_1[n]}^T\mathbf{x}\mathbf{x}^T\mathbf{w}_{h_1[n]} - 2\mathbf{w}_{h_1[n]}^T\mathbf{x}\mathbf{b}^T\mathbf{p}_2 + \mathbf{p}_2^T\mathbf{b}\mathbf{b}^T\mathbf{p}_2], \end{aligned}$$

and differentiated with respect to $\mathbf{p}_2$,

$$\begin{aligned} \nabla_{\mathbf{p}_2} f_0 &= \mathbb{E}[-2\mathbf{w}_{h_1[n]}^T\mathbf{x}\mathbf{b}^T + 2\mathbf{p}_2^T\mathbf{b}\mathbf{b}^T] \\ &= \mathbb{E}[-2\mathbf{w}_{h_1[n]}^T\mathbf{x}\mathbf{x}^T\mathbf{A} + 2\mathbf{p}_2^T\mathbf{A}\mathbf{x}\mathbf{x}^T\mathbf{A}] \\ &= -2\mathbf{w}_{h_1[n]}^T\mathbb{E}[\mathbf{x}\mathbf{x}^T]\mathbf{A} + 2\mathbf{p}_2^T\mathbf{A}\mathbb{E}[\mathbf{x}\mathbf{x}^T]\mathbf{A} \\ &= -2\mathbf{w}_{h_1[n]}^T\mathbf{R}\mathbf{A} + 2\mathbf{p}_2^T\mathbf{A}^T\mathbf{R}\mathbf{A}, \end{aligned}$$

Finally, imposing the partial derivative to equal zero, the optimal prediction filter is found:

$$\begin{aligned} \nabla_{\mathbf{p}_2} f_0(\mathbf{p}_2^\star) = 0 \quad &\Rightarrow \quad \mathbf{w}_{h_1[n]}^T\mathbf{R}\mathbf{A} = \mathbf{p}_2^{\star T}\mathbf{A}^T\mathbf{R}\mathbf{A} \\ &\Rightarrow \quad \mathbf{p}_2^\star = (\mathbf{A}^T\mathbf{R}\mathbf{A})^{-1}\mathbf{A}^T\mathbf{R}\mathbf{w}_{h_1[n]}. \end{aligned} \tag{3.22}$$

Once the optimal filter is found, the predicted value is

$$\hat{h}_1[n] = \mathbf{p}_2^{\star T}\mathbf{b} = \mathbf{w}_{h_1[n]}^T\mathbf{R}\mathbf{A}(\mathbf{A}^T\mathbf{R}\mathbf{A})^{-1}\mathbf{b},$$

which is the wavelet coefficient of the optimal interpolation vector (3.10) on the $\mathbf{w}_{h_1[n]}$ basis and it is the same expression as equation (3.19). This refinement of the initial PLS produces a coefficient $h_2[n] = h_1[n] - \mathbf{p}_2^{\star T}\mathbf{b}$ with lower expected energy. As discussed in §2.1.3, energy minimization is a useful criterion for image compression since wavelet-based image coders like SPIHT and EBCOT owe their performance to the efficient coding of quasi-zero energy wavelet coefficient sets.

Note that $\mathbf{p}_2^\star$ is the filter that minimizes the error of predicting a wavelet basis with the other bases and using the quadratic norm given by the correlation matrix,

$$\mathbf{p}_2^\star = \arg\min_{\mathbf{p}_2} \|\mathbf{A}\mathbf{p}_2 - \mathbf{w}_{h_1[n]}\|_{\mathbf{R}} = \arg\min_{\mathbf{p}_2} (\mathbf{A}\mathbf{p}_2 - \mathbf{w}_{h_1[n]})^T\mathbf{R}(\mathbf{A}\mathbf{p}_2 - \mathbf{w}_{h_1[n]}).$$

This construction is only a particular case of the approach. It has been assumed the solution (3.10), but others described in the previous section including more available knowledge may be used to improve results or to construct local adaptive prediction filters.

Alternatively, a coefficient $h[n]$ may be predicted using a set of scaling samples $\mathbf{l}[n]$ plus a set of its causal wavelet coefficients, denoted by $\mathbf{h}^c[n]$. Causality is imposed in order to allow synchronization between coder and decoder. Such a technique already appears in [Sai96b] with lossless compression results comparable to transforms with larger support. Including samples

of the detail channel in the prediction loop implies that the synthesis filters are IIR and not necessarily with linear phase. In the reversible integer-to-integer case quantization occurs in many places and quantization errors flow into feedback paths. In consequence, quantization errors may accumulate indefinitely. [Ada00] shows that these type of transforms show worse performance in lossy compression, but their results improve as the bit-rate increases.

The prediction with feedback is introduced in the interpolative setting conveniently ordering the matrix and vector components: the linear constraint independent term vector becomes $\mathbf{b}^T = (\mathbf{l}^T\ \mathbf{h}^{cT})$ and the system matrix becomes $\mathbf{A} = (\mathbf{W_l}\ \mathbf{W_{h^c}})$.

3.3.3 Linear Update Steps Construction

The approach offers considerable design flexibility. The same type of construction is applied to the ULS. It has been proved that solution (3.10) leads to the solution of the problem (3.21). This last expression is properly modified to derive useful ULS. The new objective functions consider the l^2-norm of the gradient (in §3.3.3.1 and §3.3.3.2) and the detail signal energy (in §3.3.3.3) in order to obtain linear ULS applicable to a set of images sharing similar statistics.

The gradient as optimization criterion is not found in literature. It only appears in some works to construct space-varying predictions [Li02, Ger06], updates [Abh03a], and in the adaptive lifting framework for the construction of ULS (e.g, [Pie01a]).

The idea behind the gradient criterion is to obtain a smooth approximate signal that leads to a better prediction performance in the subsequent resolution level. The goal is related to the usual running average preserving ULS. Also, it should be pointed out that the objective of the ULS in [Pie01a] or in [Abh03a] is the opposite: to preserve salient image structures at the lower resolution level (while low-pass filtering the homogeneous regions). These schemes amount to lower resolution image representations with more significant information, but this does not necessarily imply better compression.

The objective function in §3.3.3.2 is the gradient l^2-norm of the approximation signal $\mathbf{l}_1$ samples. Meanwhile, the objective in §3.3.3.1 is a simplified version, because it only considers the gradient with the neighbors $\mathbf{l}_0$. The consequence of this simplification is twofold: the resulting design is simpler and it allows the same interpretation relying on the optimal interpolation as in the (3.19) PLS. Thus, the different interpolation types in §3.2 as well as the local adaptive techniques may be introduced in this first ULS design. The third objective function (in §3.3.3.3) aims to design an ULS with the same goal as the prediction steps, i.e., the energy minimization. In this sense, both lifting steps work in the same direction.

Provided that a coefficient $l[n]$ is updated by means of a set of detail signal samples (which are denoted by vector $\mathbf{h}[n]$), the linear constraint system matrix is $\mathbf{A} = \mathbf{W_h}$ and the independent

term vector is $\mathbf{b} = \mathbf{h}$.

3.3.3.1 First Linear ULS Design

In the first design, the objective function is set to be the l^2-norm of the substraction between the updated coefficient $l_1[n]$,

$$l_1[n] = l_0[n] + \tilde{l}_1[n] = l_0[n] + \mathbf{u}_1^T\mathbf{b},$$

and the set $\mathcal{I}$ of the neighboring scaling coefficients. Coefficient $l_0[n]$ is updated with the quantity $\tilde{l}_1[n] = \mathbf{u}_1^T\mathbf{b}$. The goal is to find the optimal $\mathbf{u}_1^\star$ such that

$$\mathbf{u}_1^\star = \arg\min_{\mathbf{u}_1} f_0(\mathbf{u}_1),$$

with

$$f_0(\mathbf{u}_1) = \mathbb{E}\left[\sum_{i\in\mathcal{I}}(l_0[i] - (l_0[n] + \tilde{l}_1[n]))^2\right]. \tag{3.23}$$

The assumption is that the objective function leads to smooth approximate signals that help the prediction to perform better in the next resolution level. The objective function (3.23) is developed,

$$\begin{aligned}
f_0(\mathbf{u}_1) &= \sum_{i\in\mathcal{I}}\mathbb{E}\left[(l_0[i] - (l_0[n] + \tilde{l}_1[n]))^2\right] \\
&= \sum_{i\in\mathcal{I}}\mathbb{E}\left[(\mathbf{w}_{l_0[i]}^T\mathbf{x} - \mathbf{w}_{l_0[n]}^T\mathbf{x} - \mathbf{u}_1^T\mathbf{b})^2\right] \\
&= \sum_{i\in\mathcal{I}}\mathbb{E}\Big[\mathbf{w}_{l_0[i]}^T\mathbf{x}\mathbf{x}^T\mathbf{w}_{l_0[i]} + \mathbf{w}_{l_0[n]}^T\mathbf{x}\mathbf{x}^T\mathbf{w}_{l_0[n]} + \mathbf{u}_1^T\mathbf{b}\mathbf{b}^T\mathbf{u}_1 \\
&\qquad -2\mathbf{w}_{l_0[n]}^T\mathbf{x}\mathbf{x}^T\mathbf{w}_{l_0[i]} + 2\mathbf{w}_{l_0[n]}^T\mathbf{x}\mathbf{b}^T\mathbf{u}_1 - 2\mathbf{w}_{l_0[i]}^T\mathbf{x}\mathbf{b}^T\mathbf{u}_1\Big],
\end{aligned}$$

and differentiated with respect to $\mathbf{u}_1$. Then, linear constraints are introduced and the definition of correlation matrix used,

$$\begin{aligned}
\nabla_{\mathbf{u}_1} f_0 &= \sum_{i\in\mathcal{I}}\mathbb{E}\Big[2\mathbf{u}_1^T\mathbf{b}\mathbf{b}^T + 2\mathbf{w}_{l_0[n]}^T\mathbf{x}\mathbf{b}^T - 2\mathbf{w}_{l_0[i]}^T\mathbf{x}\mathbf{b}^T\Big] \\
&= 2\sum_{i\in\mathcal{I}}\mathbb{E}\Big[\mathbf{u}_1^T\mathbf{A}^T\mathbf{x}\mathbf{x}^T\mathbf{A} + \mathbf{w}_{l_0[n]}^T\mathbf{x}\mathbf{x}^T\mathbf{A} - \mathbf{w}_{l_0[i]}^T\mathbf{x}\mathbf{x}^T\mathbf{A}\Big] \\
&= 2\sum_{i\in\mathcal{I}}\mathbf{u}_1^T\mathbf{A}^T\mathbf{R}\mathbf{A} + \mathbf{w}_{l_0[n]}^T\mathbf{R}\mathbf{A} - \mathbf{w}_{l_0[i]}^T\mathbf{R}\mathbf{A},
\end{aligned}$$

and finally the derivative equalled to zero

$$\nabla_{\mathbf{u}_1} f_0(\mathbf{u}_1^\star) = 0 \quad \Rightarrow \quad |\mathcal{I}|\mathbf{u}_1^T\mathbf{A}^T\mathbf{R}\mathbf{A} = -|\mathcal{I}|\mathbf{w}_{l_0[n]}^T\mathbf{R}\mathbf{A} + \sum_{i\in\mathcal{I}}\mathbf{w}_{l_0[i]}^T\mathbf{R}\mathbf{A}.$$

Let denote the mean of the neighboring approximate signal basis vectors as

$$\overline{\mathbf{w}}_{\mathcal{I}} = \frac{1}{|\mathcal{I}|} \sum_{i \in \mathcal{I}} \mathbf{w}_{l_0[i]}.$$

Then, the optimal update filter minimizing the local gradient is

$$\mathbf{u}_1^\star = (\mathbf{A}^T\mathbf{R}\mathbf{A})^{-1}\mathbf{A}^T\mathbf{R}(\overline{\mathbf{w}}_{\mathcal{I}} - \mathbf{w}_{l_0[n]}), \tag{3.24}$$

and the optimally updated coefficient is

$$l_1[n] = l_0[n] + \tilde{l}_1[n] = l_0[n] + \mathbf{u}_1^{\star T}\mathbf{b} = l_0[n] + (\overline{\mathbf{w}}_{\mathcal{I}} - \mathbf{w}_{l_0[n]})^T\mathbf{R}\mathbf{A}(\mathbf{A}^T\mathbf{R}\mathbf{A})^{-1}\mathbf{b}. \tag{3.25}$$

Interestingly, if $\overline{\mathbf{w}}_{\mathcal{I}} = \mathbf{0}$, then (3.25) computes the minimum l^2-norm of the gradient of $l_1[n]$ w.r.t. the zero vector, which is equivalent to minimize the energy. In this case, the optimal update reduces to the optimal prediction of (3.22). Again, the interpretation relying on the optimal interpolation of $\mathbf{x}$ is possible:

$$l_1[n] = l_0[n] + \mathbf{u}_1^{\star T}\mathbf{b} = l_0[n] + (\overline{\mathbf{w}}_{\mathcal{I}} - \mathbf{w}_{l_0[n]})^T\mathbf{x}^\star,$$

since it allows the use of additional knowledge for the design. Therefore, interpolation methods that fit into the PLS goals are equivalently useful for the construction of new ULS.

A related design is developed in the next section. Note that the proposal is not restricted to the construction of first updates $\mathbf{u}_1$. It is also a design for intermediate or final ULS.

3.3.3.2 Second Linear ULS Design

An additional consideration on the set of approximate signal neighbors $\mathcal{I}$ may be included in the previous gradient-minimization design. As each sample in $\mathcal{I}$ is also updated, it is interesting to consider the minimization of the gradient of $l[n] + \tilde{l}[n]$ with respect to the updated samples $l[i] + \tilde{l}[i]$, $i \in \mathcal{I}$, through a still unknown update filter. To this goal, the objective function (3.23) is modified in order to find the optimal update with this criterion. The objective function is

$$f_0(\mathbf{u}_1) = \mathbb{E}\left[\sum_{i \in \mathcal{I}} (l_1[i] - l_1[n])^2\right] = \mathbb{E}\left[\sum_{i \in \mathcal{I}} ((l_0[i] + \tilde{l}_1[i]) - (l_0[n] + \tilde{l}_1[n]))^2\right].$$

Taking into account that the updated coefficient basis vector is

$$\mathbf{w}_{l_1[i]} = \mathbf{w}_{l_0[i]} + \mathbf{A}_{l_0[i]}\mathbf{u}_1,$$

being $\mathbf{A}_{l_0[i]}$ the constraint matrix relative to the position of sample $l_0[i]$ and $\mathbf{A} = \mathbf{A}_{l_0[n]}$, the objective function results

$$f_0(\mathbf{u}_1) = \mathbb{E}\left[\sum_{i \in \mathcal{I}} (\mathbf{w}_{l_0[i]}^T\mathbf{x} + \mathbf{u}_1^T\mathbf{A}_{l_0[i]}^T\mathbf{x} - \mathbf{w}_{l_0[n]}^T\mathbf{x} - \mathbf{u}_1^T\mathbf{A}^T\mathbf{x})^2\right],$$

which is expanded to

$$\begin{aligned} f_0(\mathbf{u}_1) \;=\; \sum_{i\in\mathcal{I}} \mathbb{E}\Big[& \mathbf{w}_{l_0[i]}^T\mathbf{x}\mathbf{x}^T\mathbf{w}_{l_0[i]} + \mathbf{u}_1^T\mathbf{A}_{l_0[i]}^T\mathbf{x}\mathbf{x}^T\mathbf{A}_{l_0[i]}\mathbf{u}_1 + 2\mathbf{w}_{l_0[i]}^T\mathbf{x}\mathbf{x}^T\mathbf{A}_{l_0[i]}\mathbf{u}_1 \\ & + \mathbf{w}_{l_0[n]}^T\mathbf{x}\mathbf{x}^T\mathbf{w}_{l_0[n]} + \mathbf{u}_1^T\mathbf{A}^T\mathbf{x}\mathbf{x}^T\mathbf{A}\mathbf{u}_1 - 2\mathbf{w}_{l_0[n]}^T\mathbf{x}\mathbf{x}^T\mathbf{w}_{l_0[i]} - 2\mathbf{w}_{l_0[n]}^T\mathbf{x}\mathbf{x}^T\mathbf{A}_{l_0[i]}\mathbf{u}_1 \\ & + 2\mathbf{w}_{l_0[n]}^T\mathbf{x}\mathbf{x}^T\mathbf{A}\mathbf{u}_1 - 2\mathbf{w}_{l_0[i]}^T\mathbf{x}\mathbf{x}^T\mathbf{A}\mathbf{u}_1 - 2\mathbf{u}_1^T\mathbf{A}_{l_0[i]}^T\mathbf{x}\mathbf{x}^T\mathbf{A}\mathbf{u}_1\Big], \end{aligned}$$

and introducing the definition of $\mathbf{R}$,

$$\begin{aligned} f_0(\mathbf{u}_1) \;=\; \sum_{i\in\mathcal{I}} \mathbb{E}\Big[& \mathbf{w}_{l_0[i]}^T\mathbf{R}\mathbf{w}_{l_0[i]} + \mathbf{u}_1^T\mathbf{A}_{l_0[i]}^T\mathbf{R}\mathbf{A}_{l_0[i]}\mathbf{u}_1 + 2\mathbf{w}_{l_0[i]}^T\mathbf{R}\mathbf{A}_{l_0[i]}\mathbf{u}_1 \\ & + \mathbf{w}_{l_0[n]}^T\mathbf{R}\mathbf{w}_{l_0[n]} + \mathbf{u}_1^T\mathbf{A}^T\mathbf{R}\mathbf{A}\mathbf{u}_1 - 2\mathbf{w}_{l_0[n]}^T\mathbf{R}\mathbf{w}_{l_0[i]} - 2\mathbf{w}_{l_0[n]}^T\mathbf{R}\mathbf{A}_{l_0[i]}\mathbf{u}_1 \\ & + 2\mathbf{w}_{l_0[n]}^T\mathbf{R}\mathbf{A}\mathbf{u}_1 - 2\mathbf{w}_{l_0[i]}^T\mathbf{R}\mathbf{A}\mathbf{u}_1 - 2\mathbf{u}_1^T\mathbf{A}_{l_0[i]}^T\mathbf{R}\mathbf{A}\mathbf{u}_1\Big]. \end{aligned}$$

Differentiating this expression w.r.t. $\mathbf{u}_1$ leads to

$$\begin{aligned} \nabla_{\mathbf{u}_1} f_0 \;=\; 2\sum_{i\in\mathcal{I}} \Big[& \mathbf{u}_1^T\mathbf{A}_{l_0[i]}^T\mathbf{R}\mathbf{A}_{l_0[i]} + \mathbf{w}_{l_0[i]}^T\mathbf{R}\mathbf{A}_{l_0[i]} + \mathbf{u}_1^T\mathbf{A}^T\mathbf{R}\mathbf{A} \\ & - \mathbf{w}_{l_0[n]}^T\mathbf{R}\mathbf{A}_{l_0[i]} + \mathbf{w}_{l_0[n]}^T\mathbf{R}\mathbf{A} - \mathbf{w}_{l_0[i]}^T\mathbf{R}\mathbf{A} - 2\mathbf{u}_1^T\mathbf{A}_{l_0[i]}^T\mathbf{R}\mathbf{A}\Big]. \end{aligned}$$

Equalling the expression to zero and denoting the mean of the different products of the basis vectors and matrices as

$$\begin{aligned} \overline{\mathbf{A}}_{\mathcal{I}} &= \frac{1}{|\mathcal{I}|}\sum_{i\in\mathcal{I}} \mathbf{A}_{l_0[i]}, \\ \overline{\mathbf{R}}_{\mathcal{I}} &= \frac{1}{|\mathcal{I}|}\sum_{i\in\mathcal{I}} \mathbf{A}_{l_0[i]}^T\mathbf{R}\mathbf{A}_{l_0[i]}, \\ \overline{\mathbf{b}}_{\mathcal{I}} &= \frac{1}{|\mathcal{I}|}\sum_{i\in\mathcal{I}} \mathbf{A}_{l_0[i]}^T\mathbf{R}\mathbf{w}_{l_0[i]}, \end{aligned}$$

then, the optimal solution is described by

$$\mathbf{u}_1^\star = \left(\mathbf{A}^T\mathbf{R}(\mathbf{A} - 2\overline{\mathbf{A}}_{\mathcal{I}}) + \overline{\mathbf{R}}_{\mathcal{I}}\right)^{-1}\left(\mathbf{A}^T\mathbf{R}(\overline{\mathbf{w}}_{\mathcal{I}} - \mathbf{w}_{l_0[n]}) + \overline{\mathbf{A}}_{\mathcal{I}}^T\mathbf{R}\mathbf{w}_{l_0[n]} - \overline{\mathbf{b}}_{\mathcal{I}}\right). \tag{3.26}$$

This expression of awkward appearance is simple to compute in practice, since the only difference w.r.t. (3.24) are the additional terms concerning the neighbors basis vectors means, which are known and fixed if the previous prediction step is a fixed classical PLS.

3.3.3.3 Third Linear ULS Design

A third type of ULS construction is proposed. The PLS is assumed to be the same linear filter through all resolution levels. The objective function is set to be the prediction error energy of the next resolution level. Thus, the prediction filter is employed to determine the basis vectors as

well as the subsequent prediction error. The ULS is assumed to be the last of the decomposition. The updated samples $l_L^{(1)}[n]$ are split into even $l_L^{(1)}[2n]$ and odd $l_L^{(1)}[2n+1]$ samples that become the new approximation $l_0^{(2)}[n] = l_L^{(1)}[2n]$ and detail $h_0^{(2)}[n] = l_L^{(1)}[2n+1]$ signals, respectively. For simplicity, L is set to 1 in the following. In the next resolution level, the odd samples are predicted by the even ones and the ULS design aims to minimize the energy of this prediction. It is also assumed that the same update filter is used for even and odd samples. Therefore, the objective function is

$$f_0(\mathbf{u}_1) = \mathbb{E}\left[(l_1[2n+1] - \mathbf{p}_1^T\mathbf{l}_1[2n])^2\right] = \mathbb{E}\left[(l_0[2n+1] + \tilde{l}_1[2n+1] - \mathbf{p}_1^T(\mathbf{l}_0[2n] + \tilde{\mathbf{l}}_1[2n]))^2\right].$$

The prediction filter length determines the number of even samples $l_1[2i]$ employed by the prediction. These samples appear in the column vector $\mathbf{l}_1[2n]$ as

$$\mathbf{l}_1[2n] = \begin{pmatrix} \vdots \\ l_1[2n] \\ l_1[2n+2] \\ \vdots \end{pmatrix}.$$

Respecting this notation, the objective function results in

$$f_0(\mathbf{u}_1) = \mathbb{E}\left[\left(\mathbf{w}_{l_0[2n+1]}^T\mathbf{x} + \mathbf{u}_1^T\mathbf{A}_{l_0[2n+1]}^T\mathbf{x} - \mathbf{p}_1^T\left(\begin{pmatrix} \vdots \\ \mathbf{w}_{l_0[2n]}^T \\ \mathbf{w}_{l_0[2n+2]}^T \\ \vdots \end{pmatrix}\mathbf{x} + \begin{pmatrix} \vdots \\ \mathbf{u}_1^T\mathbf{A}_{l_0[2n]}^T \\ \mathbf{u}_1^T\mathbf{A}_{l_0[2n+2]}^T \\ \vdots \end{pmatrix}\mathbf{x}\right)\right)^2\right].$$

Employing the prediction filter taps

$$\mathbf{p}_1^T = (\ \ldots \quad p_{1,i-1} \quad p_{1,i} \quad p_{1,i+1} \quad \ldots\ )$$

the expression is set in a summation form

$$f_0(\mathbf{u}_1) = \mathbb{E}\left[\left(\mathbf{w}_{l_0[2n+1]}^T\mathbf{x} + \mathbf{u}_1^T\mathbf{A}_{l_0[2n+1]}^T\mathbf{x} - \sum_i p_{1,i}\mathbf{w}_{l_0[2(n+i)]}^T\mathbf{x} - \sum_i p_{1,i}\mathbf{u}_1^T\mathbf{A}_{l_0[2(n+i)]}^T\mathbf{x}\right)^2\right].$$

First, this expression is expanded. Then, the definition of $\mathbf{R}$ is used. Afterwards, the resulting expression is differentiated w.r.t. the vector $\mathbf{u}_1$, reaching the expression

$$\begin{aligned}
\nabla_{\mathbf{u}_1} f_0(\mathbf{u}_1) \;=\;& 2\mathbf{u}_1^T\mathbf{A}_{l_0[2n+1]}^T\mathbf{R}\mathbf{A}_{l_0[2n+1]} + 2\mathbf{w}_{l_0[2n+1]}^T\mathbf{R}\mathbf{A}_{l_0[2n+1]} \\
+\;& 2\sum_i\sum_k p_{1,i}p_{1,k}\mathbf{u}_1^T\mathbf{A}_{l_0[2(n+i)]}^T\mathbf{R}\mathbf{A}_{l_0[2(n+k)]} - 2\sum_i p_{1,i}\mathbf{w}_{l_0[2(n+i)]}^T\mathbf{R}\mathbf{A}_{l_0[2n+1]} \\
+\;& 2\sum_i\sum_k p_{1,i}p_{1,k}\mathbf{w}_{l_0[2(n+i)]}^T\mathbf{R}\mathbf{A}_{l_0[2(n+k)]} - 2\sum_i p_{1,i}\mathbf{w}_{l_0[2n+1]}^T\mathbf{R}\mathbf{A}_{l_0[2(n+i)]} \\
-\;& 4\sum_i p_{1,i}\mathbf{u}_1^T\mathbf{A}_{l_0[2(n+i)]}^T\mathbf{R}\mathbf{A}_{l_0[2n+1]}.
\end{aligned}$$

Finally, it is equalled to zero and the optimal filter is derived. Being the notation similar to the precedent design,

$$\begin{aligned} \mathbf{A} &= \mathbf{A}_{l_0[2n+1]}, \\ \overline{\mathbf{w}}_p &= \sum_i p_{1,i} \mathbf{w}_{l_0[2(n+i)]}, \\ \overline{\mathbf{A}}_p &= \sum_i p_{1,i} \mathbf{A}_{l_0[2(n+i)]}, \end{aligned}$$

the optimal update filter is expressed as

$$\mathbf{u}_1^\star = \left(\mathbf{A}^T \mathbf{R} \left(\mathbf{A} - 2\overline{\mathbf{A}}_p \right) + \overline{\mathbf{A}}_p^T \mathbf{R} \overline{\mathbf{A}}_p \right)^{-1} \left(\mathbf{A} - \overline{\mathbf{A}}_p \right)^T \mathbf{R} \left(\overline{\mathbf{w}}_p - \mathbf{w}_{l_0[2n+1]} \right). \tag{3.27}$$

The final expression (3.27) is similar to the filter (3.26) obtained in the previous design. However, the optimal filter emerging from this design differs from the previous one even in the simple case that it has two taps and the prediction is $\mathbf{p}_1 = \begin{pmatrix} 1/2 & 1/2 \end{pmatrix}^T$. For larger supports, the difference is more remarkable. These facts are analyzed in the experiments section.

3.4 Experiments

This section explains several experiments to prove practical applications of the developed framework. Some considerations concerning the interpolation methods are reported in §3.4.2. The formulation derived for the linear lifting filters is employed in two ways. First, as a tool to analyze existing filters optimality in §3.4.3. The basis example is the LeGall 5/3 wavelet, but the same approach is possible for any wavelet filter factorized into lifting steps. Second in §3.4.4, the formulation is used to enhance LS by improving lifting steps and adding new ones according to image or image class statistics. The new decompositions are applied to signal coding and image compression.

An estimation or a model of the auto-correlation matrix $\mathbf{R}$ is required in the global optimization approaches. Images are assumed to be an auto-regressive process of first-order (AR-1) or second-order (AR-2) in most of the experiments. The auto-regressive model is specified in §3.4.1. The explicit auto-correlation matrix construction is also provided.

3.4.1 Auto-regressive Image Model

An auto-regressive model is a linear modeling of a discrete process based on the assumption that each value of the process depends only on a weighted sum of the previous values plus noise. Mathematically, an AR-m model for the output $x[n]$ is

$$x[n] = \sum_{i=1}^{m} a_i x[n-i] + \eta[n],$$

Image Class	Natural	Synthetic	Texture	Mammo.	SST	MOC
Mean	0.9701	0.9434	0.8569	0.9564	0.9953	0.9936
Std. dev.	0.0710	0.0686	0.1105	0.0479	0.0015	0.0074

Table 3.1: Mean value and standard deviation of the ρ parameter for each image class.

Image Class	Natural	Synthetic	Texture	Mammo.	SST	MOC
a_1	1.0688	0.8958	0.6671	0.9374	1.1583	0.7993
a_2	-0.0993	0.0676	0.2410	0.0198	-0.1637	0.1949

Table 3.2: AR-2 parameters mean value for each image class.

where a_i for $1 \leq i \leq m$ are the auto-regressive parameters and η is the noise. In the AR-1 case, parameter a_1 is usually denoted by ρ and it is called auto-correlation coefficient or AR-1 parameter.

The auto-regressive parameters may be estimated from the image data through the Yule-Walker equations or the least squares method, among other techniques. The estimation may be done for a whole image class, for a specific image, or even for a region or line in an image. Furthermore, the AR parameters may be tuned according to the statistics of each filtering direction. The parameter estimation scope determines the resulting filter range of applicability.

In the AR-1 case, matrix $\mathbf{R}$ is completely determined by parameter ρ. The mean and standard deviation of ρ for each image class is shown in table 3.1. Appendix A describes the corpus of images employed in the experimental part. Once ρ is obtained, matrix entries are $[\mathbf{R}]_{i,j} = \rho^{|i-j|}$, for $0 \leq i, j \leq n-1$ and $|\rho| < 1$. The AR-1 parameter is in the range $0.95 < \rho < 1$ for all classes of images except for the textures class that it is $\rho \simeq 0.86$.

In the AR-2 case, matrix $\mathbf{R}$ is determined by the second-order parameters a_1 and a_2. The estimated AR-2 parameters for various image classes are found in table 3.2. Matrix $\mathbf{R}$ is a Toeplitz matrix and so, it is completely specified by its first row. Element $[\mathbf{R}]_{1,1}$ is set to 1 and $[\mathbf{R}]_{1,2} = \frac{a_1}{1-a_2}$. The recursion equation

$$[\mathbf{R}]_{1,j} = a_1[\mathbf{R}]_{1,j-1} + a_2[\mathbf{R}]_{1,j-2},$$

for $j > 2$ gives the rest of the row elements.

3.4.2 Interpolation Methods

This part §3.4.2 is devoted to a qualitative assessment of the proposed interpolation methods. Three reasons impel to a non-exhaustive experimental setting. First, the power of these type of interpolation is partly known. The approach is constructed on the work [Mur04], which successfully apply a local adaptive interpolation equivalent to the optimal solution given by (3.8).

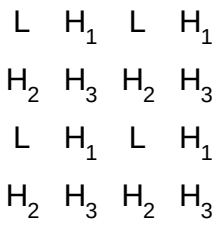

Figure 3.2: 2-D grid with a 4-band sampling.

Second, since the dissertation addresses the lifting scheme, the emphasis is put on the new lifting designs performance in §3.4.3 and §3.4.4. The third reason is a practical one. The proposed quadratic interpolation formulation is very rich and offers many different variants. The number of experiments to test all the possible variants is huge because they should contemplate the points in the list below, which also explain the basic setting for the qualitative assessment.

- The method is able to construct 1-D separable or directly 2-D interpolations. In the latter case, the strategy is to split the input image in four bands as shows figure 3.2. Once the samples are partitioned in the so-called L, H_1, H_2, and H_3 bands, the H_3 samples are first interpolated using the other three bands, which are included as linear constraints. Then, the H_2 samples are interpolated using the L and H_1 ones as reference and linear constraints. Finally, the H_1 band is interpolated with L band samples, leading to an approximation signal, and the three detail signals formed by the three bands of prediction errors. This is a simple way to the interpolate employing much of the available information and the one used to obtain the results given below to assess the methods performance. Other strategies may be considered. Alternatives are the use of a quincunx grid or the prediction error feedback in the interpolation of the H_1 and H_2 bands.

- As stated, the formulation accepts local and global settings.

  - *Global* means that the same quadratic class is selected for the whole image. In this case, the image model should be chosen.
  - For the local adaptive interpolation, the local patches size and support have to be selected. In the experiments below, the choice is 4x4 and 8x8, respectively (like in figure 3.1). Furthermore, an initial interpolation is required. Different choices exist to this goal, being the bi-linear and the bi-cubic interpolations the preferred ones. Finally, the patches may be extracted from other similar images or images from the same class.

- The interpolation method output may be re-introduced in the algorithm as an initial interpolation. The number of iterations may affect the final result and it should be determined.

The experiments below do not iterate if nothing else is stated. Usually, one or two iterations improve the initial results, but the performance tends to decrease in the subsequent iterations.

- Six interpolation methods are articulated in section 3.2, each of which may behave differently on each image class.
- In addition, some of the methods are parameter-dependant:
  - The signal regularized and the energy penalizing approaches balance two different objective functions according to a parameter (defined as γ and δ, respectively) that have to be specified.
  - The weighting objective matrix $\mathbf{W}$ in (3.13) should be defined by the application or the image at hand. The distance weighting depends on the image type, e.g., a textured image with a repeated pattern requires different weights than a highly non-stationary image.

Clearly, the casuistry is important, but a general trend may be drawn. The interpolation given by (3.8) has a better global behavior than the others; it outperforms the other methods and it reduces the 5/3 wavelet detail signal energy from 5% to 20% for natural, synthetic, and sea surface temperature (SST) images. The results are poorer for the mammography and the textures.

The weighted objective interpolation (3.13) attains very similar results to the (3.8), being better is some cases. For instance, the interpolation error energy is around 3% smaller for the texture image set.

The signal bound constraint (3.11) may be useful for images with a considerable amount of high-frequency content, as the synthetic and SST classes. Some interpolation coefficients outside the bounds appear for these kind of images, and thus, the method rectifies them. However, there is no energy reduction and certainly a computational cost increase w.r.t. (3.8).

The signal regularized solution (3.17) performs very well with small values of δ that give a lower weight to the regularizing factor w.r.t. the $\mathbf{c}$ vector l^2-norm objective. Interestingly, in the 1-D case and with a difference matrix $\mathbf{D}$ relating all the neighboring samples, the objective factor $\|\mathbf{Dx}\|^2$ coincides with $\mathbf{x}^T\mathbf{R}^{-1}\mathbf{x}$ being $\mathbf{R}$ the auto-correlation matrix of an AR-1 process with $\rho \to 1$. Therefore, the signal regularized method may be seen as an interpolation mixing local signal knowledge with an image model.

The inclusion of the energy penalizing factor in the formulation did not prove to be useful for the available images set because it damages the final result. Maybe, this factor could be considered for highly-varying images like SAR images in order to avoid the apparition of extreme values.

PSNR	Bi-cubic	A - 1 it.	A - 2 it.	B - 1 it.	B - 2 it.	C - 1 it.
Baboon	22.447	22.459	22.395	22.468	22.433	**22.522**
Barbara	24.647	24.084	23.653	24.253	23.905	**24.756**
Cheryl	35.299	35.414	35.361	35.433	**35.438**	33.940
Farm	22.439	22.658	22.736	22.647	**22.737**	21.416
Girl	34.355	34.538	**34.610**	34.518	34.586	33.072
Lena	33.973	34.255	**34.385**	34.226	34.349	32.147
Peppers	**32.020**	31.724	31.776	31.881	31.839	30.962

Table 3.3: Interpolation PSNR from down-sampled images using the bi-cubic, the basic quadratic interpolation of (3.8) (column noted by A) and the distance weighted objective (B) with 1 and 2 iterations, and the regularized signal objective (C) with 1 iteration.

PSNR	Bi-cubic	A - 1 it.	A - 2 it.	B - 1 it.	B - 2 it.	C - 1 it.
Baboon	22.356	**23.810**	23.695	23.717	23.745	23.595
Barbara	24.296	25.653	25.741	25.610	25.753	**25.831**
Cheryl	32.736	34.161	**34.819**	34.091	34.759	33.620
Farm	20.539	22.265	**22.490**	22.176	22.486	21.963
Girl	31.693	33.232	**34.034**	33.147	33.936	32.762
Lena	30.606	32.107	**33.058**	32.049	32.960	31.583
Peppers	29.875	31.105	31.573	31.149	**31.648**	30.775

Table 3.4: Interpolation PSNR from the averaged and down-sampled images using the bi-cubic, the basic quadratic interpolation (A) and the distance weighted objective (B) with 1 and 2 iterations, and the regularized signal objective (C) with 1 iteration.

3.4.2.1 Interpolation Methods PSNR Performance

The interpolation methods are further assessed with the ensuing experiment. The bi-cubic interpolation serves as benchmark and the comparison criterion is the PSNR, defined as

$$\text{PSNR} = 10 \log_{10} \left(\frac{255^2}{\text{MSE}} \right).$$

Table 3.3 shows some results concerning the natural images with 512x512 pixels of appendix A. Images are down-sampled by a factor of 2 without anti-aliasing filter, and then the down-sampled image is re-interpolated using different methods and number of iterations. Their performance tend to be quite similar to that of the bi-cubic interpolation. Certainly, there are many interpolation methods that outperform these ones, but the interest of the proposed methods resides in the inclusion of additional low-pass filtering constraints and in their application to lifting design. Following variation of the experiment resembles more to the lifting setting. Table 3.4 shows the results for the case that each pixel is the average of four high-density pixels before the down-sampling. Performance in terms of PSNR is better than the bi-cubic interpolation.

In addition of the PSNR performance, the resulting interpolated images are less blurry and

sharper around the existing edges if the adequate set of parameters is selected.

However, the interpolation goal for this dissertation is the lifting steps construction. The assumption that from a good interpolation arises good PLS as well as good first design ULS is made. Another important aspect is the derivation of closed-form LS, which is a desirable property in most of the applications due to its significantly lower computational cost. Following sections deal with lifting steps performance.

3.4.3 Optimality Analysis

The LeGall 5/3 wavelet introduced in §2.2.4 is analyzed through the point of view given by the optimal lifting steps derived in section 3.3.

The LeGall 5/3 low-pass or scaling basis vectors have the form

$$\mathbf{w}_{l_1[n]} = (\ \ldots \quad 0 \quad -1/8 \quad 2/8 \quad 6/8 \quad 2/8 \quad -1/8 \quad 0 \quad \ldots\ )^T,$$

being equal to the $\mathbf{0}$ vector except for the locations from $2n-2$ to $2n+2$. Meanwhile, the high-pass or wavelet basis vectors have the form

$$\mathbf{w}_{h_1[n]} = (\ \ldots \quad 0 \quad 0 \quad -1/2 \quad 1 \quad -1/2 \quad 0 \quad 0 \quad \ldots\ )^T,$$

being the $\mathbf{0}$ vector except for the positions $2n$, $2n+1$, and $2n+2$. The prediction lifting filter is $\mathbf{p}_1 = (\ 1/2 \quad 1/2\ )^T$ and the update lifting filter is $\mathbf{u}_1 = (\ 1/4 \quad 1/4\ )^T$. In the following, such filters are denoted by $\mathbf{p}_{LG}$ and $\mathbf{u}_{LG}$, respectively.

The optimality of $\mathbf{u}_{LG}$ is studied in §3.4.3.2 according to the three ULS designs and the AR image model. The ULS are derived for the prediction $\mathbf{p}_{LG}$. For fair comparison, the proposed ULS employ two neighbors as the $\mathbf{u}_{LG}$ filter. Therefore, in practice the application simply reduces to propose a coefficient different from 1/4 for the update filter (since it is symmetric). The proposals attain noticeable improvements even in this simple case. Also, several considerations on $\mathbf{p}_{LG}$ are formulated in §3.4.3.1. Finally, second PLS according to expression (3.20) are presented in §3.4.3.3 assuming the initial $\mathbf{p}_{LG}$ and $\mathbf{u}_{LG}$. These PLS are optimized for each image class. Some of the resulting basis vectors are given. Results are compared to those of two other known 5/11 transforms.

Notice that the type of analysis described in the following may be applied to any existing transform via lifting scheme.

3.4.3.1 First Prediction Step Study

One of the simplest applications of the stated linear lifting framework design is the prediction of $h_0[n]$ with the samples $l_0[n]$ and $l_0[n+1]$. Which is the best way of doing such a prediction?

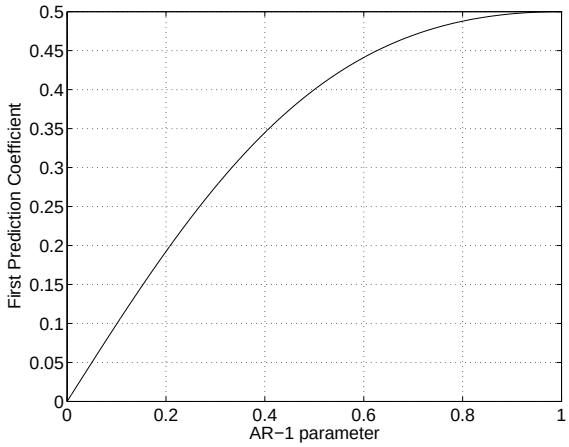

Figure 3.3: Optimal prediction filter as function of the AR-1 parameter using 2-taps and the design (3.20).

Intuitively, the answer is $\mathbf{p}_1 = \mathbf{p}_{LG}$, or at most, a linear combination of $l_0[n]$ and $l_0[n+1]$ with coefficients summing up to one. Spectral considerations and vanishing moments also point to the LeGall 5/3 prediction as the best choice. However, the proposed prediction (3.20) gives different answers depending on the auto-correlation matrix $\mathbf{R}$.

Basis vectors $\mathbf{w}_{l_0[n]}$, $\mathbf{w}_{h_0[n]}$, and $\mathbf{w}_{l_0[n+1]}$ are composed of zeros except one 1 at the position $2n$, $2n+1$, and $2n+2$, respectively. These vectors are plugged into (3.20) and the optimal $\mathbf{p}_1$ is derived assuming an AR-1 image model. The prediction filter depends on the parameter ρ as figure 3.3 shows. When $\rho \to 1$, the optimal prediction tends to the intuitive $\mathbf{p}_{LG}$. Data is highly correlated and so, its projection onto the vectors $\mathbf{w}_{l_0[n]}$ and $\mathbf{w}_{l_0[n+1]}$ is informative about the projection onto $\mathbf{w}_{h_0[n]}$, i.e., about the value of $h_0[n]$. The construction respects symmetry, leading to $\mathbf{p}_1 = \mathbf{p}_{LG}$. There is no correlation among data when $\rho = 0$, i.e., when $\mathbf{R} = \mathbf{I}$. In this case, there is no information in $l_0[n]$ and $l_0[n+1]$ about $h_0[n]$, and the expression (3.20) says that any attempt to predict the value $h_0[n]$ amounts to an MSE increase: in mean, the residual has higher energy. Intermediate coefficient values appear for $0 < \rho < 1$.

Despite these results differ from the usual $\mathbf{p}_{LG}$, the answer given by the proposal is mathematically consistent according to the image model. Therefore, a possible approach weakness is found in the image model determined by $\mathbf{R}$. An AR-1 model may be suited for many image applications as its wide use in image processing confirms, but certainly not for all. As an example, the predictor arising from the texture images case $\rho \simeq 0.86$ is $\mathbf{p}_1 = \begin{pmatrix} 0.494 & 0.494 \end{pmatrix}^T$, which leads to systematically worse results compared to $\mathbf{p}_{LG}$ despite the coefficients are very similar.

A more suitable image model seems to be the AR-2. A signal generated with an AR-2 model resembles to an image row or column much more than an AR-1 process insofar as the AR-2 parameters sum approximately to one. Figure 3.4 relates the optimal linear PLS (3.20) with the

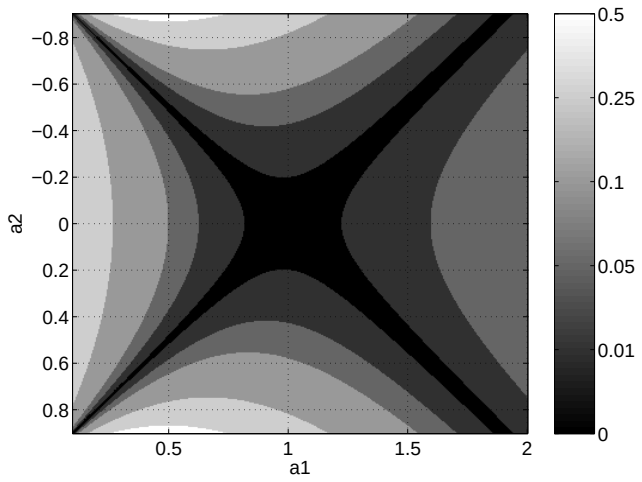

Figure 3.4: Level sets of the optimal prediction coefficient minus 0.5 as a function of the AR-2 parameters using 2-taps and the linear PLS design (3.20).

second-order auto-regressive parameters. The figure shows six level sets of the optimal prediction coefficient with respect to the a_1 and a_2 parameters. The function is the absolute value of the optimal prediction coefficient for the given parameters minus 1/2. Thus, the resulting filter is similar to $\mathbf{p}_{LG}$ in the dark areas and it is different in the light areas. Note that the gray-scale is not uniform w.r.t. the function value.

As it can be observed from the figure, the optimal PLS based on the AR-2 model is almost equal to $\mathbf{p}_{LG}$ for most part of the parameters. Indeed, prediction coefficients are 1/2 for the set $a_1 + a_2 \simeq 1$. The set $a_1 + a_2 = 1$ is relevant because an AR-2 model with these parameters preserves the sample mean expected value.

3.4.3.2 Update Step Study

Assuming an AR-1 process and the initial prediction $\mathbf{p}_{LG}$, the three linear ULS of §3.3.3 lead to coefficients depending on ρ as depicted in figure 3.5. The second and the third designs lead to similar coefficients for all the range. Meanwhile, the ULS coefficient arising from the first design is smaller for all the interval. Asymptotically ($\rho \to 1$), the second ULS design output doubles the coefficients of first and third ones. The update filter coefficients are considerably below the 1/4 reference for the three designs and the usual ρ found in practice (like the ones in table 3.1). This fact agrees with the common observation that in some cases the $\mathbf{u}_{LG}$ omission increases compression performance, being the ULS included in the decomposition process because of the multi-resolution properties improvement. The issue of the ULS employment can be approached from the perspective given by the proposed linear ULS designs: the ULS is useful, but the correct choice is an update coefficient quite smaller than 1/4 (as the three ULS indicate for the usual ρ

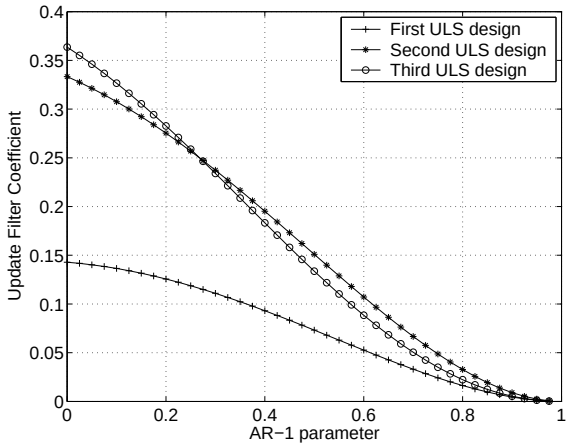

Figure 3.5: Update filter as function of the AR-1 parameter for the three ULS designs. The update is a two-tap symmetrical filter and so, it is depicted only one coefficient. The first considered prediction is the $\mathbf{p}_{LG}$.

values).

The optimal ULS for each of the three designs are also derived assuming a second-order auto-regressive model. For a subset of the AR-2 parameters, the resulting optimal update coefficients coincide with $\mathbf{u}_{LG}$, but not for other possible values. Figures 3.6 highlight this fact. For the three cases, each figure relates the optimal update coefficient according to the given criterion w.r.t. the AR-2 parameters. Six level sets of the update coefficient are depicted as a function of a_1 and a_2. From the figure, it is concluded that $\mathbf{u}_{LG}$ is far from being optimal in the sense of (3.26), (3.24), and (3.27) for many possible image AR-2 parameters. To position a practical reference, the three circles in figure 3.6b depict the mean AR-2 parameters of the synthetic, mammography, and SST image classes.

3.4.3.3 Second Prediction Step Study

The LeGall 5/3 wavelet properties may be improved by means of a second PLS. The high-pass filter support is increased to 11 taps if the PLS uses the samples

$$\mathbf{l}_1[n] = (\ l_1[n-1] \quad l_1[n] \quad l_1[n+1] \quad l_1[n+2]\ )^T.$$

The inclusion of more approximation signal samples in the second PLS is possible, but it does not assure a performance improvement, since the high-pass filter becomes very lengthy.

The 5/11-a transform via lifting in table 3.5 is proposed in [Cal98], being

$$\mathbf{p}_2 = (\ -1/16 \quad 1/16 \quad 1/16 \quad -1/16\ )^T.$$

The 5/11-a is a (4,2) transform: it has 4 analysis vanishing moments (and the 2 synthesis

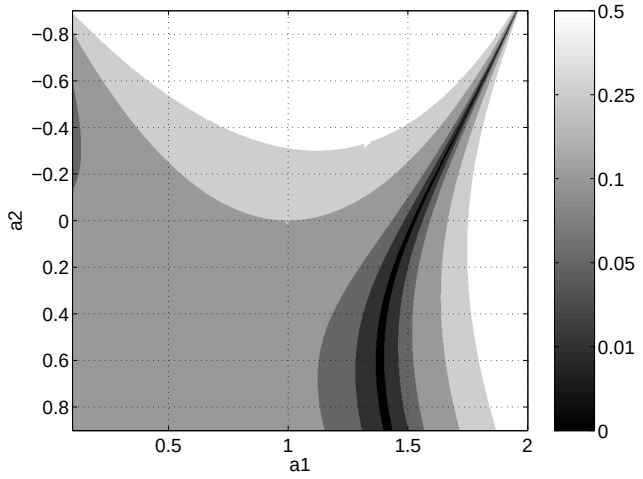

(a)

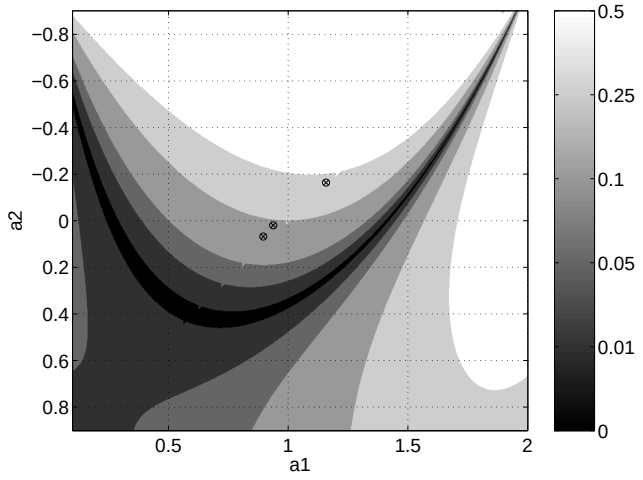

(b)

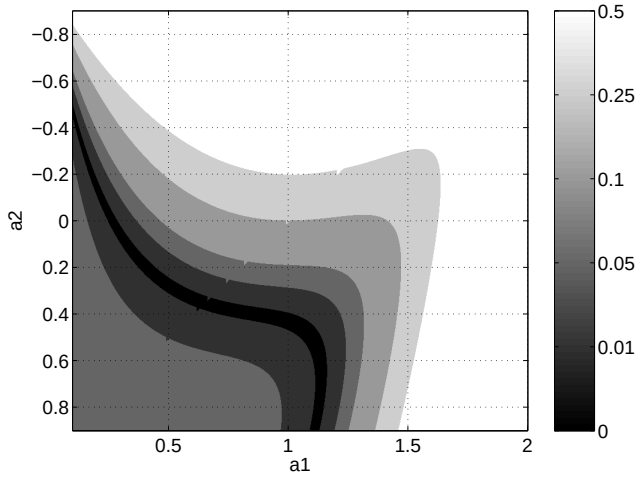

(c)

Figure 3.6: Level sets of the optimal update coefficient minus 0.25 in function of the AR-2 parameters for **(a)** the first linear ULS design, **(b)** the second linear ULS design (circles indicate the mean parameters of the synthetic, mammography, and SST image classes), and **(c)** the third linear ULS design.

Filter Name	*Lifting Steps*
5/11-a	$h_1[n] = h_0[n] - \left\lceil \frac{1}{2} l_0[n] + \frac{1}{2} l_0[n+1] \right\rfloor$ $l_1[n] = l_0[n] + \left\lceil \frac{1}{4} h_1[n-1] + \frac{1}{4} h_1[n] \right\rfloor$ $h_2[n] = h_1[n] - \left\lceil -\frac{1}{16} l_1[n-1] + \frac{1}{16} l_1[n] + \frac{1}{16} l_1[n+1] - \frac{1}{16} l_1[n+2] \right\rfloor$
5/11-b	$h_1[n] = h_0[n] - \left\lceil \frac{1}{2} l_0[n] + \frac{1}{2} l_0[n+1] \right\rfloor$ $l_1[n] = l_0[n] + \left\lceil \frac{1}{4} h_1[n-1] + \frac{1}{4} h_1[n] \right\rfloor$ $h_2[n] = h_1[n] - \left\lceil -\frac{1}{32} l_1[n-1] + \frac{1}{32} l_1[n] + \frac{1}{32} l_1[n+1] - \frac{1}{32} l_1[n+2] \right\rfloor$

Table 3.5: Lifting steps for the 5/11-a and 5/11-b transforms.

vanishing moments coming from the 5/3 structure). The 5/11-b transform in table 3.5 is proposed in [Ada99], which is designed considering several criteria (cf. §2.3.1). The filter coefficients are one-half w.r.t. the 5/11-a, being

$$\mathbf{p}_2 = (\ -1/32 \quad 1/32 \quad 1/32 \quad -1/32\ )^T.$$

The 5/11-b is a (2,2) transform, but it attains better results than the 5/11-a for images with high-frequency content.

The linear PLS (3.20) for an AR-1 model is applied to the LeGall 5/3 wavelet to obtain a second prediction and the corresponding 5/11 transform. Figure 3.7 depicts $\mathbf{p}_2$ as a function of ρ. As a reference, the horizontal grids in the graph depict the values -1/16, -1/32, 1/32, and 1/16 (which are the coefficients of the 5/11-a and 5/11-b second prediction). The graph confirms that values close to 1/16 are suitable for smoother images, and the coefficients may decrease (in absolute value) when there is more high-frequency content, i.e., when ρ moves away from one.

Another counter-intuitive effect due to the chosen image model is that prediction coefficients do not sum up to zero for small ρ values. Figure 3.7 shows this effect through the dashed line that depicts $\sum_i p_{2,i}$.

The scheme is applied to some image classes. The optimal second prediction steps $\mathbf{p}_2^\star$ using the ρ of natural, textures, and SST images are

$$\begin{aligned}
\mathbf{p}^\star_{2,natural} &= (\ -0.05960 \quad 0.05966 \quad 0.05966 \quad -0.05960\ )^T,\\
\mathbf{p}^\star_{2,texutre} &= (\ -0.05832 \quad 0.05852 \quad 0.05852 \quad -0.05832\ )^T,\\
\mathbf{p}^\star_{2,SST} &= (\ -0.05969 \quad 0.05970 \quad 0.05970 \quad -0.05969\ )^T,
\end{aligned}$$

which are close to the 5/11-a because their ρ are close to one. The corresponding underlying wavelet basis vectors are given in table 3.6.

Lifting steps have been analyzed by means of the developed framework. The following section employs the optimal steps arising from the framework in order to check their coding performance.

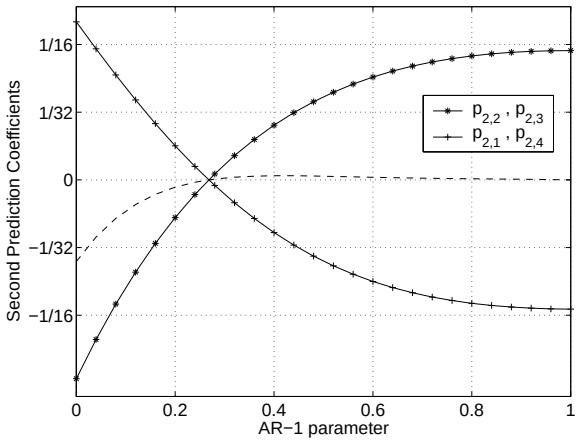

Figure 3.7: Second prediction filter $\mathbf{p}_2$ as function of the AR-1 parameter, being $\mathbf{p}_1 = \mathbf{p}_{LG}$ and $\mathbf{u}_1 = \mathbf{u}_{LG}$. The horizontal grid lines depict the coefficients of the 5/11-a and 5/11-b second prediction filter. The dashed line depicts the sum of the filter coefficients: $\sum_i p_{2,i}$.

n	$\mathbf{w_{h_2}[n]}$
0	0.97017
±1	-0.54474
±2	-0.00001
±3	0.05216
±4	0.01490
±5	-0.00745

(a)

n	$\mathbf{w_{h_2}[n]}$
0	0.97074
±1	-0.54387
±2	-0.00005
±3	0.05106
±4	0.01458
±5	-0.00729

(b)

n	$\mathbf{w_{h_2}[n]}$
0	0.97015
±1	-0.54477
±2	0
±3	0.05223
±4	0.01492
±5	-0.00746

(c)

Table 3.6: Underlying basis vectors applying the optimal second prediction step to the LeGall 5/3 wavelet, computed with the ρ for **(a)** natural, **(b)** texture, and **(c)** SST image classes.

3.4.4 Improved Linear Lifting Steps Performance

Despite the LS steps developed in this chapter allow the construction of 2-D non-separable filters, all the following experiments except one are restricted to 1-D separable decompositions. The transforms are integer-to-integer applied to lossless (image) compression.

3.4.4.1 ULS with AR-1 Signal Test

In the first experiment, the input signal is synthetic data generated to check the proposal performance for the assumed image model. An AR-1 process containing 512 samples is decomposed in three resolution levels using $\mathbf{p}_{LG}$ followed by $\mathbf{u}_{LG}$ or one of the three designed ULS. These four transforms are compared by computing the gradient l^2-norm of $\mathbf{l}_1^{(1)}$ and the $\mathbf{h}_1^{(2)}$ signal mean energy, which are the second and third ULS objective functions. Figures 3.8 and 3.9 show the

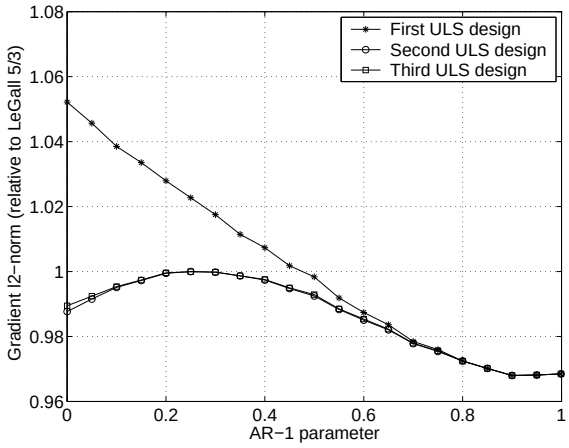

Figure 3.8: Relative gradient of $\mathbf{l}_1$ for the optimal ULS w.r.t. LeGall 5/3.

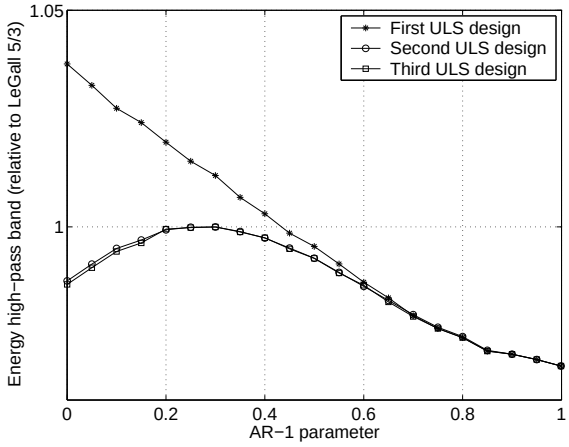

Figure 3.9: Relative energy of $\mathbf{h}_1^{(2)}$ for the optimal ULS w.r.t. LeGall 5/3.

mean results for 1000 trials. The relative gradient and energy of the three ULS w.r.t. the LeGall 5/3 wavelet are depicted.

Second and third design are almost equal and outperform LeGall 5/3 in terms of energy and gradient for all ρ except for $\rho \simeq 0.27$; value for which the three design coefficients coincide. The first design shows worse performances, in particular for the case of small ρ. However, this design has more flexibility and may incorporate additional knowledge that leads to a better image model.

The given results are obtained with an additive white gaussian noise of a standard deviation equal to 50. The relative gradient and energy are weak functions of the AR process noise variance. The weighted entropy has also been computed, but it is a function sensitive to the noise variance. However, a qualitative conclusion may be drawn: entropy is higher for the LeGall 5/3 w.r.t. the

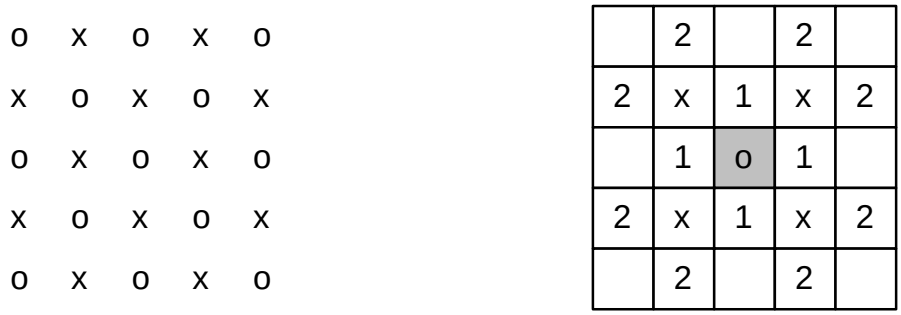

(a) (b)

Figure 3.10: (a) A rectangular grid divided into two quincunx grids (marked 'o' and 'x'). **(b)** PLS support on quincunx grid. Pixel at site 'o' is predicted with pixels at sites '1' (if a 4-tap filter is used) and also with pixels at sites '2' (if a 12-tap filter is employed). Pixels at sites 'x' perform the 4-tap prediction at the next resolution level.

second and third design for ρ near 1. On the contrary, LeGall 5/3 attains better entropies for ρ close to 0.

3.4.4.2 ULS on a Quincunx Grid with AR Data

This second experiment contributes a lifting construction example of a non-separable wavelet on a quincunx grid. A 2-D rectangular grid may be down-sampled into two quincunx grids (figure 3.10a), which become the approximation and detail signals.

The derivation of ULS on the quincunx lattice within the developed framework is more involving than the 1-D separable case. The underlying basis vectors are two dimensional and their support is larger than the 1-D case. The 2-D basis must be mapped into 1-D vectors to match the linear LS setting. Also, the number of neighboring samples employed for the filtering is greater. These facts complicate the implementation, especially for large filter supports. Therefore, this experiment is restricted to small supports: the prediction of a pixel at site 'o' employs the first ring of neighbors, which are the ones indicated in figure 3.10b with a '1'. The considered prediction filter coefficient is 1/4 for the four neighbors. This filter is known as the second-order Neville filter [Kov00]. The subsequent 4-tap ULS vanishing 2 moments uses the coefficient 1/8, i.e., the update filter is

$$\mathbf{u}_{nv} = (\ u_N \quad u_E \quad u_S \quad u_W\ )^T = (\ 1/8 \quad 1/8 \quad 1/8 \quad 1/8\ )^T,$$

following the notation of figure 3.11a. Larger prediction supports may been considered (e.g., [Kov00]). For instance, the sites marked '2' in the figure 3.10b may be included in the PLS, like in the fourth-order Neville filter.

The third ULS design leads to minimize the subsequent prediction error energy. Thus, it is preferred that the ULS is immediately followed by the PLS of the next resolution level instead

(a) (b)

Figure 3.11: (a) Support and notation for the 4-tap ULS on the quincunx grid. **(b)** Typical geometry of a 2-D auto-regressive neighborhood. Four pixels are used for generating the pixel at site 'o'.

of the filtering in the horizontal/vertical direction as it happens in the 1-D separable case. The two-band quincunx grid permits this. The neighbors employed in next resolution PLS are marked with a cross in figure 3.10b. The linear constraint matrix for each of these four coefficients is plugged into equation 3.27 to obtain the optimal ULS. The filters have the restriction $u_N = u_S$ and $u_E = u_W$ by the directional symmetry of the construction and by the auto-correlation matrix structure.

As in the previous experiment, the input signal is synthetic data generated according to an auto-regressive model. Four neighboring pixels are considered for the predictive model as figure 3.11b shows. The constraint $\sum_{i=1}^{4} a_i = 1$ is imposed. Images with 512x512 pixels are generated. A 3-level quincunx decomposition is computed using the 4-tap prediction with coefficient 1/4 and the optimal ULS. For comparison, images are also decomposed with the second-order Neville filter. The comparison criterion is again the $\mathbf{h}_1^{(2)}$ signal mean energy. The decomposition is performed by means of a modified version of the Matlab® LISQ toolbox [Zee02].

In contrast with the 1-D case, the non-separable optimal third ULS design does not perform consistently better than the reference filter. The result depends on the AR signal orientation. If the signal has a dominant horizontal feature ($a_1 \approx 1$ and $a_2, a_3, a_4 \approx 0$), the update filter is

$$\mathbf{u} = (\ -0.4645 \quad -0.9435 \quad -0.4645 \quad -0.9435\ )^T,$$

which is very different from $\mathbf{u}_{nv}$ and it remarkably reduces the $\mathbf{h}_1^{(2)}$ energy around a 99%. The same behavior appears when the dominant direction is the vertical, but interchanging the filter coefficient values. Results worsen when the dominant direction moves away the horizontal or vertical directions. The worst results appear when the dominant direction is 45° (e.g., $a_1, a_3 = 1/2$ and $a_2, a_4 = 0$). In this case, the third ULS design increase the second-order Neville $\mathbf{h}_1^{(2)}$ energy around a 15%. The update filter turns out to be

$$\mathbf{u} = (\ 0.3418 \quad 0.3474 \quad 0.3418 \quad 0.3474\ )^T,$$

that is, the design points out a filter with equal-valued coefficients like $\mathbf{u}_{nv}$, but this value is significantly higher, and it damages the final performance compared to $\mathbf{u}_{nv}$. Maybe the approach

Rate (bpp)	5/3 wavelet	AR-1 model
Synthetic	3.832	3.508
SST	3.252	3.123
Mammography	2.349	2.358

Table 3.7: Compression results with JPEG2000 using the standard LeGall 5/3 wavelet and the proposed optimal update with the AR-1 model for the synthetic, mammography, and SST image classes. Results are given in bits per pixel.

should also contemplate a constraint on the filter coefficients or other considerations in order to avoid this drawback.

Given this performance disparity, the proposed quincunx ULS may be employed in practice in a space-varying setting which determines the dominant signal direction triggering the use of the proposed ULS in the favorable cases and the Neville filter otherwise.

3.4.4.3 Local Adaptive ULS

This experiment is described in [Sol06a]. An AR-2 model is used to determine the local image behavior. A line-wise space-varying update filter is constructed by estimating the AR-2 parameters for each line in the image using the filter given by (3.26). To assess the performance, the energy of the coarser level detail coefficients $\mathbf{h}_1^{(2)}$ is computed. For the set of natural images, the energy is up to 25% smaller for the space-varying optimal update step w.r.t. $\mathbf{u}_{LG}$.

3.4.4.4 Image Class Optimal ULS Test

This fourth experiment (also appeared in [Sol06a]) derives filters applicable to a more global setting. The AR-1 parameter is estimated for three image classes. Therefore, the model is useful for a whole corpus of images instead of being local. Synthetic, mammography, and SST images are used. Each corpus contains 15 images. The correlation matrix is determined by the AR-1 parameter (in table 3.1), and it is plugged into equation (3.24) in order to obtain an update filter used for all the images in a class. Image compression is performed with a four resolution level decomposition within the JPEG2000 coder environment. Numerical results appear in table 3.7 compared to the LeGall 5/3 wavelet. The proposal compression results improve those of the LeGall 5/3 for the synthetic and SST image classes, but results slightly worsen for the mammography class. The latter case is analyzed in the next experiment.

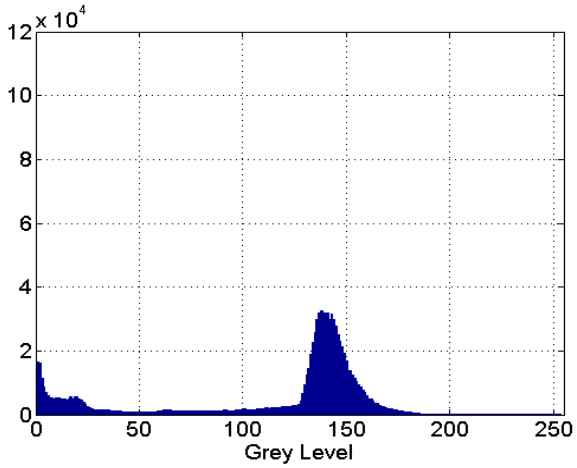

Figure 3.12: A mammography image histogram.

3.4.4.5 A Refinement for Mammography

The optimal ULS (3.24) results in experiment of §3.4.4.4 are worse for the mammography image class w.r.t. the LeGall 5/3 wavelet. The reason may be found in the formation of this kind of images. Clearly, there are two differentiated regions: an homogenous dark one containing the background and a light heterogeneous foreground. Figure 3.12 is the histogram of a mammography. There is an accumulation of light pixels between the 100 and 200 gray level due to the foreground. Background pixels are found at the smaller values, typically less than 50. Most part of background pixels accumulate around the 0 gray level (which is difficult to distinguish in the histogram figure).

Background and foreground have distinct auto-correlation and AR parameters. The mean of both AR parameters is not optimal for any of the two regions. A more accurate approach for this class should contemplate an AR model or derive an auto-correlation matrix for each of the regions separately. Thus, an image segmentation is required.

The histogram inspection suggests the following segmentation algorithm. As the gray level almost characterizes the two regions, a binary image is formed by thresholding at the gray level $T = 50$. The resulting binary image has two differentiated regions with some pixels placed in the wrong part. A morphological opening with a disk of radius 5 as the structuring element corrects the misplaced pixels. Two distinguished and connected regions constitute the final segmentation. Figure 3.13 shows the initial image and the segmentation. This threshold plus opening segmentation algorithm is simple and obtains crude results compared to many other techniques, but the output is good enough for the experiment purposes.

Using the segmented binary image as a mask, the auto-correlation matrix is directly estimated for each region, as well as the AR-2 parameters. Then, the optimal ULS are derived.

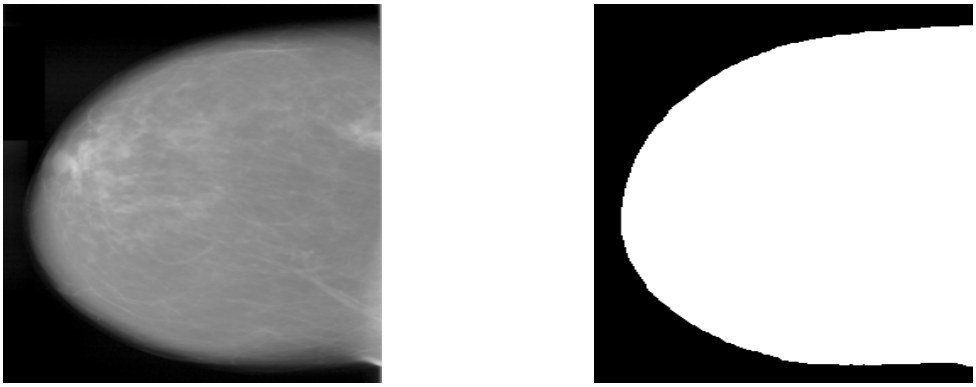

(a) (b)

Figure 3.13: (a) A mammography and **(b)** the segmentation in background and foreground.

Both auto-correlation matrices lead to similar update coefficients. For instance, the third design coefficient for the background using the AR-2 auto-correlation matrix is 0.12584 and the coefficient using the direct estimation of $\mathbf{R}$ is 0.12053. Second and third designs attain very similar coefficients, while the first design coefficient tends to be one half of them. This was proved in the analysis of §3.4.3 for the AR-1 case when $\rho \to 0$. With the direct correlation estimation, second linear ULS background coefficient is 0.13209 and the foreground coefficient is 0.02430. Meanwhile, for the third design the background coefficient is 0.12053 and the foreground coefficient is 0.02456.

In view of these results, dyadic coefficients are used for the mammography coding: $1/8 = 0.1250$ for the background and $1/32 = 0.03125$ for the foreground. Therefore, the background and foreground filters are $\mathbf{u}_b = (\ 1/8 \quad 1/8\ )^T$ and $\mathbf{u}_f = (\ 1/32 \quad 1/32\ )^T$, respectively.

Once the coefficients are determined, the image decomposition does not require any mask. The prediction is followed by a space-varying ULS that depends on the next approximation coefficient value. If this coefficient is greater than the threshold T, it means that the region is foreground an the $\mathbf{u}_f$ filter is employed. Otherwise, the region is considered to be background and the optimal filter for the background $\mathbf{u}_b$ is used:

$$l_1[n] = \begin{cases} l_0[n] + \mathbf{u}_f^T \mathbf{h}_1[n], & \text{if } l_0[n+1] > T, \\ l_0[n] + \mathbf{u}_b^T \mathbf{h}_1[n], & \text{otherwise,} \end{cases}$$

The decoder has to take into account this coding modification in order to be synchronized w.r.t. the coder and to decide the filter according to the same data.

Image compression is again performed with a four resolution level decomposition within the JPEG2000 coder environment. The mean results for the 15 mammography decreases from 2.358 bpp to 2.336 bpp.

Rate (bpp)	5/3 wavelet	5/11-a	5/11-b	Opt. P AR-1	Opt. P AR-2
Synthetic	3.832	4.044	4.011	4.036	4.027
SST	3.252	3.317	3.288	3.312	3.329
Mammography	2.349	2.349	2.348	2.349	2.347

Table 3.8: Compression results with JPEG2000 using the standard LeGall 5/3 wavelet, the 5/11-a, the 5/11-b, and the optimal second prediction according to the AR-1 and AR-2 models for the synthetic, mammography, and SST image classes.

3.4.4.6 Optimal Second PLS Test

Second prediction optimal design is tested using the AR-1 and AR-2 models for each image class. Results are given in table 3.8 for 4 resolution level decompositions.

In all cases, the optimized second prediction is a filter with coefficients in between the 5/11-a and the 5/11-b ones. This is due to the image model and the estimated parameters (table 3.1 and 3.2). Both models attain similar results. The performance tends to be better for the 5/11-b, which would arise in the optimized prediction setting for smaller ρ than the estimated ones. Furthermore, the 5/3 wavelet performs significantly better.

These results coincide with the findings in [Ada00]: in lossless compression the 5/3 transform yields to better results than the 5/11 transforms for images with relatively greater amount of high-frequency content, often by a considerable gap. The 5/3 wavelet implies $\rho \approx 0.27$ in the AR-1 model, which is far from the estimated parameters.

The 5/11 transforms outperform the 5/3 in lossy compression and in lossless compression for natural imagery [Ada00]. This observation is consistent with our experiment using the 512x512 natural images. They are decomposed in 4 resolution levels and compressed with EBCOT. Results appear in table 3.9. The optimized second prediction for the image class (columns "O.P. AR-1" and "O.P. AR-2") yields to similar results for both models, and almost equal to those of the 5/11-a.

The model may be computed for each image. The rates attained by the AR-1 model are given in the column headed by "AR-1 Im.". Results are also similar to the 5/11-a transform because $0.9 \leq \rho < 1$. Further adaptation may be conceived. For instance, the optimal second prediction may be computed for each resolution level in the image. In this case, the mean rate is 4.633 bpp with the AR-1 model. Even more, images may be partitioned and the optimal prediction estimated for each part, like in the works [BB03, Hat04, Hat05] that use a quadtree structure to convey the partition. Book-keeping may be required depending on the estimation procedure. The trend is that performance improves when the model is better matched to the data.

Rate (bpp)	**5/3 wav.**	**5/11-a**	**5/11-b**	**O.P. AR-1**	**O.P. AR-2**	**AR-1 Im.**
Baboon	6.109	6.092	6.091	6.093	6.092	6.093
Barbara	4.776	4.691	4.723	4.691	4.685	4.691
Cheryl	2.442	2.414	2.425	2.415	2.415	2.415
Farm	6.426	6.402	6.407	6.403	6.403	6.402
Girl	3.956	3.938	3.937	3.936	3.937	3.935
Lena	4.314	4.284	4.285	4.280	4.284	4.281
Peppers	4.625	4.627	4.617	4.626	4.632	4.626
Mean	4.664	4.635	4.641	4.635	4.635	4.635

Table 3.9: Compression results with JPEG2000 using the standard LeGall 5/3 wavelet, the 5/11-a, the 5/11-b, and the optimal second prediction according to the AR-1 and AR-2 models for a set of seven natural images of 512x512 pixels.

3.5 Chapter Summary and Conclusions

This chapter develops a linear framework employed to derive new lifting steps. The point of departure is a quadratic interpolation method from which several alternatives are given. The conclusion regarding the proposed methods is that their performance in terms of PSNR is around 1.5 dB better than the bi-cubic interpolation when the image being interpolated has been low-pass filtered before the down-sampling. However, the final result depends on the appropriate choice of the interpolation method and its parameters to the image at hand.

In a natural way, the initial interpolation formulation is used for the LS design by adding an extra set of linear equality constraints. This permits the design of PLS minimizing the detail signal energy and the design of ULS with approximation signal gradient criteria. Indeed, the given optimal interpolation obtained with any of the precedent methods may be applied to create new PLS and ULS.

The framework is also employed for an optimality analysis of the LeGall 5/3 wavelet according to the established criteria. The main conclusion is that there are image classes for which this commonly used wavelet is not optimal. The compression results within the JPEG2000 environment confirm this observation. Also in this case, a correct choice of the image model and parameters is required to obtain the best results.

Finally, the lifting design framework flexibility is demonstrated with the variety of described experiments. Different image models are used to derive lifting steps on quincunx grid, space-varying ULS, first and second PLS, line-wise adaptive ULS, and the two ULS for the mammography.

This chapter concludes the research contribution made in the linear lifting scheme. Chapter 4 and 5 address the lifting scheme design and optimization from a nonlinear perspective.